

THE DYNAMIC STATE OF  
WHILLANS ICE STREAM, WEST ANTARCTICA

A Thesis

Presented in Partial Fulfillment of the Requirements for  
the Degree Master of Sciences in the  
Graduate School of The Ohio State University

By

Leigh Asher Stearns, B.A.

\* \* \* \* \*

The Ohio State University  
2002

Master's Examination Committee:

Dr. Kenneth C. Jezek, Adviser

Dr. C.J. van der Veen

Dr. James Downs

Dr. Carolyn Merry

Approved by

---

Adviser  
Department of Geological Sciences

## ABSTRACT

This paper investigates changes that are occurring on the Whillans Ice Stream using two velocity data sets. Velocities derived from photogrammetry in 1985-1989 yield information about the state of the ice stream ten years ago. These results are compared to interferometric (InSar) velocities from 1997.

Four different methods of analysis were conducted to assess how Whillans Ice Stream is changing. First, the temporal and spatial changes in velocity, shear stress and strain rate were determined by comparing the two data sets. Second, the mass balance of the ice stream in 1988 and in 1997 was determined. Third, the force budget of the ice stream was determined. Finally, the orientation of flowlines derived from a 1963 DISP image was compared to the orientation of flowlines in the Radarsat 1997 image.

All four of these techniques indicate that substantial changes of Whillans Ice Stream have occurred in the past ten years. The ice stream is decelerating over time. It is also thickening at the down-stream end and may be experiencing an increase in basal drag. Extending the observations back to 1963 highlights even more dramatic changes. In 1963, WIS2 was the dominant tributary, pinching out WIS1 as the two tributaries merged. In 1997, the reverse is occurring. WIS2 is getting pinched out by WIS1 as they merge.

This paper describes the changes that are observed and calculated by comparing the aforementioned velocity data sets. Hypothetical causes for these changes are then discussed.

Dedicated to my mother, for her worries.

AND

In memory of the two men who would have enjoyed reading this the most:

Ian M. Whillans (1944 - 2001) and Richard B. Stearns (1937 – 1993).

## ACKNOWLEDGMENTS

This project was completed thanks to the encouragement and wisdom of many. A special thanks to Ken Jezek who introduced me to remote sensing and who generously supported me over the past year. I would also like to thank Kees van der Veen for dealing with my incessant questioning and math deficiencies with good humor. Gordon Hamilton kept me on the track of glaciology by providing me with fieldwork opportunities and by (patiently) teaching me many field skills. Members of the Remote Sensing Lab and fellow students at the Byrd Polar Research Center and in the Geology Department taught me a lot about glaciology and geology through various discussions and lectures.

This work was inspired by Ian Whillans who first brought attention to the enigmatic nature of Ice Stream B (now Whillans Ice Stream). His leadership, wisdom and sense of humor are greatly missed.

This research was supported by NASA grant NAG5-10275.

## VITA

May 24, 1977 .....Born – New York, NY

1999 .....B.A. Geology, Carleton College

1999 – present .....Graduate Research Assistant, The Ohio State University

## FIELDS OF STUDY

Major Field: Geological Sciences

## TABLE OF CONTENTS

Abstract.....	ii
Dedication.....	iv
Acknowledgments.....	v
Vita.....	vi
List of Figures.....	x
List of Tables.....	xii
Chapters:	
1. Introduction.....	1
1.1 Study Motivation.....	1
2. Background.....	4
2.1 Mass Balance Studies.....	4
2.2 Glaciological Setting and Force Budget.....	6
2.2.1 Physical Characteristics of Whillans Ice Stream.....	7
2.2.2 Mechanical Controls of Whillans Ice Stream.....	9
2.2.2.1 Basal Mechanics.....	9
2.2.2.2 Longitudinal Stresses.....	13
2.2.2.3 Lateral Drag.....	13
2.3 Ice Stream Morphology.....	14
2.4 Project Objectives.....	15
3. Data Collection.....	16
3.0 Overview.....	16
3.1 InSAR Data.....	16
3.1.0 Overview.....	16
3.1.1 Data Acquisition and Processing.....	17
3.1.2 Application of InSAR Data.....	19

3.2 Photoblock Data.....	20
3.2.0 Overview.....	20
3.2.1 Data Acquisition.....	22
3.2.2 Data Processing.....	23
3.2.3 Photoblock Accuracy.....	24
3.3 Radarsat Imagery.....	26
3.3.0 Overview.....	26
3.3.1 Data Processing.....	27
3.4 Declassified Intelligence Satellite Photography.....	27
3.4.0 Overview.....	27
3.4.1 Data Processing.....	28
3.5 Bed Topography (BEDMAP).....	31
3.6 Surface Topography (OSUDEM).....	31
3.7 Accumulation Rates.....	33
3.8 Compilation of Data Sets.....	33
4. Spatial and Temporal Changes in Flow Dynamics.....	38
4.1 Introduction.....	38
4.2 Velocity Variations.....	38
4.2.1 Spatial Variations in Velocity.....	38
4.2.2 Temporal Variations in Velocity and Flow Direction.....	41
4.2.2.1 Velocity Variations.....	41
4.2.2.2 Flow Direction Variations.....	42
4.3 Shear Strain Rate Variations.....	44
4.3.1 Spatial Variations in Shear Strain Rate.....	46
4.3.2 Temporal Variations in Shear Strain Rate.....	47
4.4 Shear Stress Variations.....	47
4.4.1 Spatial Variations in Shear Stress.....	49
4.4.2 Temporal Variations in Shear Stress.....	49
4.5 Implications/Explanations.....	50
5. Mass Balance and Force Budget.....	51
5.0 Goals.....	51
5.1 Mass Balance.....	51
5.1.1 Equations.....	52
5.1.2 Error Estimates.....	57
5.1.3 Mass Balance Results.....	58
5.1.3.1 Tributary B2.....	61
5.1.3.2 Tributary B1.....	63
5.1.3.3 Whillans Ice Stream.....	64

5.2 Force Budget Technique.....	66
5.2.1 Driving Stress.....	68
5.2.2 Longitudinal Tension / Compression.....	70
5.2.3 Lateral Drag.....	71
5.2.4 Basal Drag.....	72
5.2.5 Spatial Changes in the Force Budget.....	74
5.2.6 Temporal Changes in the Force Budget.....	75
5.3 Conclusions.....	75
6. Conclusions.....	77
References.....	80
Appendix A: Photoblock Orientation.....	85
Appendix B: Mass Balance Results.....	86

## LIST OF FIGURES

FIGURE		PAGE
1	The location of the Ross Ice Streams shown on a Radarsat image.....	2
2	Geometry of cross-track interferometric SAR.....	18
3	InSAR velocities for Whillans Ice Stream. Velocities under 50 m/yr and areas with no data are shaded gray. Thick black lines spanning across the ice stream represent flux gates used in the mass balance calculation. Thin black lines trending down the ice stream represent flowlines.....	20
4	Location of Photoblocks overlain on an InSar velocity field map.....	21
5	Cross-correlation of the InSar and photoblock data sets. a). An overlay of the two velocities (Insar and Photoblock) along transect G2a. b). Cross-correlation result for the two velocity profiles in 5a.....	25
6	Radarsat mosaic of Antarctica and the location of Whillans Ice Stream.....	26
7	The outline of the DISP images used for coverage of Whillans Ice Stream. The location of the tie points and ground control points used to register the DISP images are shown as well.....	30
8	Radarsat image, Surface DEM and Bedrock Topography of Whillans Ice Stream.....	32
9	Velocity profiles along Whillans Ice Stream. The solid red lines represent InSAR velocities. The blue dots represent measured photoblock data points; the line connecting them is interpolated. Both velocities refer to the left-and y-axis. The dashed black line is ice thickness, represented by the y-axis on the right.....	33
10	Spatial and temporal changes in velocity along Whillans Ice Stream.....	39
11	Comparison of DISP (blue) and Radarsat flowlines (red) overlain on a Radarsat image of Whillans Ice Stream.....	43

12	Shear strain rate variations across Whillans Ice Stream. Dashed blue Lines represent Photoblock results, red lines are InSAR results.....	45
13	Shear stress variations across Whillans Ice Stream. Red lines are from InSAR results; dashed blue lines are Photoblock results.....	48
14	Illustration of terms used in equation (5).....	53
15	Vertical temperature profiles relative to the basal melting point, for a ridge and an ice stream (adapted from Jacobson and Raymond, 1998).....	54
16	Flux rates (cm/yr) calculated using Photoblock velocities.....	59
17	Flux rates (cm/yr) calculated using InSar velocities.....	60
18	Temporal changes in mass balance along WIS2.....	62
19	Temporal changes in mass balance along WIS1.....	62
20	The velocity profile (smooth black line) used in this study, derived from photogrammetry compared to the velocity profile used in Shabtaie and Bentley's (1988) mass balance investigation (red line). The bullets indicate the actual data points used in their study.....	65
21	The location of resistive forces opposing glacier flow.....	67
22	Distribution of the driving stress along Whillans Ice Stream. The driving stress was calculated for each area of the ice stream, as delineated by the transverse lines.....	69
23	OSUDEM of Whillans Ice Stream, showing a substantial surface depression that trends up WIS2 from the down-stream end of the ice stream.....	79

## LIST OF TABLES

TABLE	PAGE
1	Characteristics of Argon.....28
2	Definition of terms in equation (3).....55
3	Melt rate calculated for sections of WIS.....56
4	Estimates of flux of Whillans Ice Stream.....64
5	Force Budget along Whillans Ice Stream in 1988 and 1997.....73
A1	Photoblock Information.....85
B1	Photoblock mass balance variables. <b>Fi</b> is the flux in through the up-stream gate ( $10^{12}$ kg/yr), <b>S</b> is the surface area in between the two flux gates ( $10^6$ m <sup>2</sup> ), <b>Fs</b> is the flux through the ice surface (accumulation rate times the surface area) ( $10^{10}$ kg/yr), <b>Fin</b> is the sum of Fi and Fs, <b>Fout</b> is the flux out of the down-stream gate, <b>Fnet</b> is the net flux (Fin minus Fout) ( $10^{12}$ kg/yr), and <b>H</b> is the rate of thickness change (cm/yr).....87
B2	InSar mass balance variables. <b>Fi</b> is the flux in through the up-stream gate ( $10^{12}$ kg/yr), <b>S</b> is the surface area in between the two flux gates ( $10^6$ m <sup>2</sup> ), <b>Fs</b> is the flux through the ice surface (accumulation rate times the surface area) ( $10^{10}$ kg/yr), <b>Fin</b> is the sum of Fi and Fs, <b>Fout</b> is the flux out of the down-stream gate, <b>Fnet</b> is the net flux (Fin minus Fout) ( $10^{12}$ kg/yr), and <b>H</b> is the rate of thickness change (cm/yr).....88

## CHAPTER 1

### INTRODUCTION

#### 1.1 Study Motivation

The stability of the West Antarctic Ice Sheet (WAIS) is inextricably linked to the flow mechanics of fast-flowing ice streams. Ice streams are fast moving rivers of ice that by definition, are detached from the bed (Van der Veen, 1999). The Ross Ice Streams (Figure 1) drain 40% of the ice out of the West Antarctic interior and understanding their dynamics is essential to sea level predictions (Price et al., 2000). Moreover, the West Antarctic ice streams are undergoing dynamic changes. Consequently, current sea level projections have large uncertainties because of the enormous potential and large unknowns associated with the stability of WAIS.

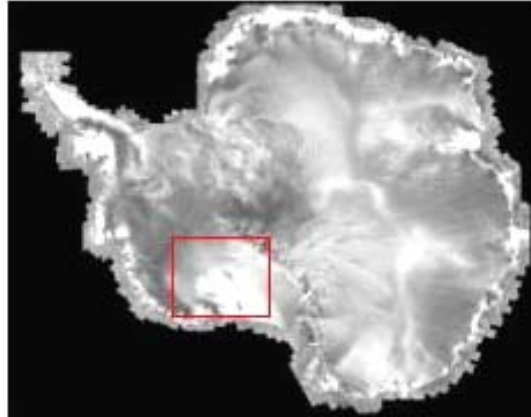


Figure 1: The location of the Ross Ice Streams shown on a Radarsat image

There is a mounting body of evidence supporting conclusions that the WAIS ice streams are evolving on century and even decadal time scales. Of the Ross Ice Streams, Ice Stream C stopped within the past century, Whillans Ice Stream is thinning, widening and decelerating, Ice Streams D and F are thickening, and Ice Stream E is thinning (Joughin et al., 2002). Rose (1979) first noticed the interaction between individual ice streams by using radio-echo sounding and Landsat imagery. He suggested that the Whillans Ice Stream was encroaching on Ice Stream C and perhaps pirating ice from its catchment, causing Ice Stream C to become quiescent. The impact that a dynamic ice stream has on its neighboring ice streams needs to be investigated in more detail.

The availability of accurate, spatially dense velocity measurements has been difficult to obtain over the Ross Ice Streams. Previous studies relied on ground-based Transit velocity measurements, which provide only point measurements of velocity. Other studies relied on airborne and satellite photography, which provide accurate data but are often limited in coverage.

Two velocity data sets are used in this study – those derived from photogrammetry and those derived from interferometry. Repeat aerial photography was obtained for four sections of Whillans Ice Stream (herein referred to as the ‘photoblocks’) in the 1985, 1986 and 1989 seasons. Velocities were derived from these photographs using manual feature tracking techniques. The velocities obtained in this manner were compared to velocities collected in 1997 from interferometry (InSAR).

This study employs three methods of analyses. First, both temporal and spatial changes in velocity were determined. Unique features in the velocity profiles were correlated to features (bedrock features, merging tributaries) observed in the Radarsat imagery. Shear stress and strain rate patterns were also investigated, for both temporal and spatial changes. Second, the state of Whillans Ice Stream was determined through mass balance calculations. The net flux of the whole ice stream was determined as was the net flux of each separate tributary (WIS1 is the southern tributary and WIS2 is the northern one). These results give insight into the patterns of mass balance change along each tributary, while also giving an overall synopsis of ice stream stability. Finally, the force budget was determined for each data set. This calculation is used to investigate the changing roles of basal and lateral drag in resisting ice stream flow. Spatial and temporal changes are correlated to observed changes in velocity and mass balance assessments.

## CHAPTER 2

### BACKGROUND

#### 2.1 Mass Balance Studies

Because the Ross Ice Streams drain approximately 40% (Price et al., 2000) of the ice out of the West Antarctic interior, numerous studies have attempted to quantify their mass balance. The mass balance is determined by comparing the mass input and the mass output in a known area. A common technique (Thomas and Bentley, 1978) is to compare discharge values through an input and output gate along the ice stream.

Shabtaie and Bentley (1988a) divided Whillans Ice Stream by seven transects and used ground-based velocity measurements to calculate the flux with the following equation.

$$F_{\text{net}} = F_i + F_r + F_l + F_S - F_b - F_{\text{out}} \quad (1)$$

Where  $F_i$  is the flux through the input gate,  $F_r$  and  $F_l$  are the fluxes through the right and left sides, respectively,  $F_S$  is the flux at the top surface (a product of the surface area,  $S$ , and the accumulation rate),  $F_b$  is the flux at the basal surface (a product of the surface area and the bottom melt rate) and  $F_{\text{out}}$  is the flux through the output gate. The basal melt

rate,  $F_b$ , is so small that it is ignored in most mass balance studies along Whillans Ice Stream (Whillans and Bindschadler, 1988; Joughin and Tulaczyk, 2002). A detailed calculation of the basal melt rate is conducted in Section 5.1.1.

Shabtaie and Bentley's results suggested that Whillans Ice Stream might be surging because of the overall patterns of flux and mass transport. According to their results there was a thinning at the catchments, an intense thinning at the head of the ice stream (where the shear margins become distinct), and a thickening in the trunk of the ice stream that diminished towards the grounding line. They estimate that Whillans Ice Stream (including the catchment area) was thinning at a rate of  $-0.12 \pm 0.02$  m/yr.

The scarcity of velocity data in Shabtaie and Bentley's mass balance calculation has encouraged subsequent mass balance estimates. Using surface velocity measurements obtained from repeat photogrammetry, Whillans and Bindschadler (1988) determined thinning rates to be  $-0.06 \pm 0.04$  m/yr for the entire ice stream (extending up to the catchment area). In addition to more precise velocity measurements, differences between these two studies reflect a refined catchment area and accumulation estimate.

The most recent estimate for the mass balance of Whillans Ice Stream is by Joughin and Tulaczyk (2002) who used Interferometric Synthetic Aperture Radar (InSAR) velocities. His results indicate that while Whillans Ice Stream may be thinning slightly, the total mass balance of all seven Ross Ice Streams is positive. This result is mostly due to Ice Stream C, which is thickening at a rate of 14 cm/yr. If a significant deceleration is occurring, as results show, then Whillans Ice Stream could be experiencing the start of a stagnant or 'binge' phase similar to Ice Stream C.

Overall, the mass balance of the Ross Ice Shelf area is spatially complex (Alley and Whillans, 1991). The inland ice is thinning at ~20% of the net accumulation rate while previous estimates for Whillans Ice Stream include thinning rates at 41% of the accumulation rate. Meanwhile, Ice Stream C is thickening at almost 100% of the accumulation rate and the Crary Ice Rise is migrating (Whillans and Van der Veen, 1993). Given this complex mass balance pattern, no simple explanation such as changes in air temperature, accumulation rate, sea level or ocean circulation could be solely responsible for these changes.

## 2.2 Glaciological Setting and Force Budget

The Antarctic Ice Sheet was much larger during the last glacial maximum (LGM), 20,000 years ago. The West Antarctic Ice Sheet is presumed to have lost 67% of its mass since the LGM, raising sea level by 11 meters. Most of this loss in mass came from a decrease in spatial extent of the ice sheet, not thickness. Where the former grounding line retreated, the Ross and Ronne/Filchner Ice Shelves were formed (Greischar and Bentley, 1980).

The ice streams leading into these ice shelves drain 40% of the ice out of WAIS and remain the most dynamic and enigmatic components of West Antarctica. The difficulties that arise when trying to understand and predict ice stream dynamics are due to the fact that ice streams are very unique and often do not follow conventional glaciological theory.

While most fast-moving glaciers sustain driving stresses of 200-300 kPa, ice streams move very fast under very small driving stresses (less than 20 kPa). Such low driving stresses are comparable to those found on ice shelves (Van der Veen, 1999).

Ever since the U.S. Siple Coast Project began in 1983, Whillans Ice Stream has been studied intensely for a variety of reasons. It was initially thought to be a prototype for West Antarctic ice streams, although the similarity of Whillans Ice Stream to its neighboring ice streams is still being investigated. In addition, Whillans Ice Stream is situated in a portion of the WAIS that is undergoing rapid changes.

### ***2.2.1 Physical Characteristics of Whillans Ice Stream***

Extending from its catchment area (defined by Price, 1998) to where it discharges into the Ross Ice Shelf, Whillans Ice Stream (WIS) is approximately 400 km long. It has a dendritic pattern of flow where four small tributaries (10-25 km wide) - WIS2a, WIS1b, WIS2a and WIS2b join - together to form the main tributaries (30-40 km wide) WIS1 and WIS2. The nearly stagnant interstream ridge that separates these two tributaries is called "The Unicorn". Down stream of the unicorn, the two tributaries coalesce to form the main trunk of the ice stream, which is approximately 50 km wide.

The low driving stress of all the Ross Ice Streams results in a concave upward longitudinal surface slope. The driving stresses are on the order of 20 kPa for the majority of WIS. Because the driving stress is small, the forces acting against it must be small as well. This implies that the bed under the ice stream is well lubricated – consisting of either a soft, deformable sediment layer or an abundance of subglacial water.

There are strong spatial velocity variations, both longitudinal and lateral, on Whillans Ice Stream. Down flow, from the upper reaches of the smaller tributaries to the trunk of the ice stream, the velocity increases ten-fold.

Lateral velocity gradients are even more dramatic. The shear margins illustrate the rapid shift in ice velocity from the slow interstream ridge to the fast-moving ice stream. Outside of the shear margin, ice is moving approximately 10 m/yr. Velocities within Whillans Ice Stream are up to 800 m/yr. The majority of the steep velocity gradient occurs in a 5-km wide zone called the shear margin. As a result, intense crevassing due to heightened strain rates defines the width of the ice stream. While the margins are distinct on the surface, there is little correlation between bed topography and margin location (Shabtaie et al., 1987a; Retzlaff et al., 1993, Joughin et al., 1999). Since the cross-sectional area directly affects the discharge volume, determining where the shear margins are and how they are evolving over time is crucial.

### *2.2.2 Mechanical Controls*

The Ross Ice Streams maintain high velocities despite surprisingly low driving stresses. While most known outlet glaciers and ice streams maintain driving stresses on the order of 200-300 kPa, the low relief of the Ross ice streams coincides with driving stresses around 20 kPa. In glacial flow, the driving stress is opposed by forces acting at the sides, at the base and at the up- and down-glacial ends (Whillans and Van der Veen, 1993). On the inland ice, the most dominant resistant stress is basal friction. On the ice streams, however, basal friction is small and most of the resistant stress emanates from the ice stream margins. The fast speeds observed on these ice streams are the product of high rates of basal motion from deformable subglacial material or slip at the base (Bentley, 1987). Since topographic constraints on ice stream location are minimal, basal processes must somehow dictate their genesis and evolution.

#### *2.2.2.1 Basal Mechanics*

As opposed to the surrounding ice, which is frozen to the bed, the base of the ice streams is at the melting point. The effective pressure (normal pressure minus water pressure) is near zero because the water is at a pressure close to the ice overburden pressure (Hooke, 1998). Such a condition is ideal for basal sliding and the deformation of soft basal sediments – both mechanisms enhancing fast glacier motion.

Two processes for explaining ice stream flow have been proposed; the more influential of the two is still being debated. The first theory suggests that basal sliding is due primarily to basal melting and therefore the location of the melting isotherm binds ice stream width (Rose et al., 1979). The second theory states that till deformation is

responsible for high basal sliding, making the ice stream bound by lithology, not thermal changes. The third theory suggests a combination of the two, based on different geologic regimes.

*1. Subglacial Materials:* To sustain high velocities under a low driving stress, the resistive force coming from the bed must be minimal. In other words, the basal sediments must be weak and deformable, unable to provide resistance to the overriding ice. Piston cores drilled to the bed of Whillans Ice Stream and Ice Streams C and D all consist of “dark gray, wet, very sticky, clay-rich diamicton that show no grading, bedding or other structure” (Kamb, 2000). Analyses of these sediments suggest that the diamicton is Tertiary glacial marine sediment that has been transported by glacier ice without detectable influence from running water. The sediment is unfrozen, soft, deformable and water saturated and sustains water-saturated bulk porosities that range from 26-58% - values that are compatible with till deformation under low effective pressures. Boreholes drilled outside the ice streams however, bring up frozen till – very different from the till underneath the ice stream. The lithology (mineralogical/petrological/paleontological components) is similar to the Whillans Ice Stream till, except that there is no (or minimal) clay component.

*2. Thermal Boundary / Basal Melting:* Ice stream existence depends heavily on the ice being at its melting point at the bed-ice interface. The fast basal motion must therefore depend on this thermal condition and small perturbations in this energy balance may trigger major rearrangements in the ice stream system (Tulaczyk et al., 2000a). In

contrast, the ice under the ice stream ridges must be below its melting point resulting in minimal (if any) basal motion. Using a model to simulate coupled heat and mass flow, Jacobson and Raymond (1998) investigated ice stream margin migrations. They found that for a morphologically uniform bed, the position of the margin is unstable and will migrate depending on the ice stream speed. If high speeds are maintained, the margins should widen by heating and entraining the adjacent ice. Conversely, a margin could migrate inward if the threshold speed is not maintained (for the Ross Ice Streams the threshold speed is  $\sim 100$  m/yr). In this case a negative heat balance at the bed would be needed in order to freeze the basal ice (Jacobson and Raymond, 1998)

*3. Subglacial Geology:* The idea that subglacial geology plays a role in the initiation of fast streaming ice is not new. When the Ross Ice Streams were first discovered it was assumed that they were directly overlying subglacial troughs. From radio-echo sounding measurements in 1988, (1988a) and Bentley disproved this theory. They found that the ice streams only roughly follow bed topography and, at times, go over subglacial ridges and are transverse to troughs. Recently, however the role of geology, not purely topography, in confining the ice streams was investigated.

As previously stated, there are essentially two theories on the mechanism of basal sliding in ice streams: deformation within the till or sliding of the ice over the till (i.e. water lubrication). Investigating the geology of the bed may provide information necessary to settle this debate. Advocates for deformable till stress the importance of saturated sediments at the base of ice streams. As a result, the ice stream must be bound either by tectonics or by erosion. Those who promote the argument for basal sliding

being a result of water lubrication or a combination of water lubrication and till deformation would expect to see a change in the geothermal heat flux confining the ice stream. Such a flux could come from a regionally thinner continental crust or contrasting thermal histories from adjacent crustal blocks.

Understanding which process of basal sliding is governing each ice stream is crucial in modeling ice streams because the till flow law and the basal sliding law are quite different. Engelhardt and Kamb (1998) attempted to separate these two components on Whillans Ice Stream using tethered stake field measurements. They found that Whillans Ice Stream velocities are dominated by high rates of basal sliding that are increasing with time. In contrast, Ice Stream D velocities are due to high rates of till deformation, not basal sliding. With seismic and aerogeophysical observations, Blankenship and others (2000) found that ice stream initiation for Ice Streams C1b and B2 depends on mid-Cenozoic sediments that are draped over the pre-existing rift-controlled topography of the embayment. In addition, local geothermal flux gradients may affect ice stream flow in these tributaries and in C1a and C2. The crust in these areas changes from the cold, thick, elevated crustal block of the Ellsworth/Whitmore Mountains to the warm, thin and depressed crust of the Ross Embayment.

#### *2.2.2.2 Longitudinal Stresses*

The interaction between ice shelves and ice stream stability has also been widely disputed. Until recently, it was hypothesized that ice shelves ‘held in’ ice streams. As a result, if the ice shelves disappeared due to global warming, WAIS would collapse. However, a force budget analysis along a flowline extending down Whillans Ice Stream to the edge of the Ross Ice Shelf (Whillans and Van der Veen, 1993b) indicated that longitudinal stress gradients were minimal.

#### *2.2.2.3 Lateral Drag*

Assuming basal drag and longitudinal stresses are small on Whillans Ice Stream, the dominant resistant force must be from lateral drag at the shear margins. Numerous studies have supported this theory (Echelmeyer et. al., 1994; Jackson and Kamb, 1997; Scambos et. al., 1994; Whillans and Van der Veen, 1997; Raymond et. al, 2000). The detailed mechanics of the force budget technique and the derivation of lateral drag will be described in Chapter 4.

### 2.3 Ice Stream Morphology

Another technique used to estimate the stability of ice streams is to compare their geometry over time. Since the discharge volume depends on the mean speed and the cross-sectional area, a change in ice stream width could greatly change the discharge flux. Different approaches to measuring shear margin migrations have shown that Whillans Ice Stream is indeed migrating. This discovery carries implications not only for changes in ice flux, but also for understanding ice stream mechanics.

First of all, if shear margins migrate with fluidity, then the control on their location must be transient as well (i.e., they are not confined by bedrock topography). In addition, since resistance provided by basal drag is minimal for most of Whillans Ice Stream, resistance from the sides must counteract the driving stress (Whillans and Van der Veen, 1993). For areas where this is the case, the speed of the ice stream should be proportional to the fourth power of the width. Under these circumstances a positive feedback loop could continuously entrain slow-moving ridge ice into the ice stream, thus progressively widening it. Such a process would cause an exponential increase in ice discharge (assuming the ice stream did not thin as it widened).

To test this hypothesis and to determine the stability of Whillans Ice Stream, its shear margins have been studied extensively using various theoretical and field measurements. Velocity profiles (Echelmeyer and Harrison, 1998), crevasse curvature methods (Hamilton and Whillans, 1998) and theoretical studies (Jacobsen and Raymond, 1998) all suggest a  $\sim 7$  m/yr outward migration of the southern margin of ISB2. Van der Veen and Whillans (1996) developed a simple model that describes the relationship between the lateral drag and basal drag as an ice stream changes width. Their study

highlights the importance of understanding how ridge ice is entrained into the ice stream. Unfortunately, it is difficult to make conclusions for the whole area based on point measurements and models, which is why remote sensing techniques are so important. Bindschadler and Vornberger (1998) compared aerial photographs from 1963 to AVHRR imagery from 1992. Their results reveal changes much greater than previously suggested with an outward migration rate of  $137 (\pm 34)$  m/yr and a concomitant decrease in velocity by 50%. More comparisons using remote sensing techniques need to be made for the whole ice stream before its stability is properly assessed.

#### 2.4 Project Objectives

There are essentially three methods used to determine the stability of a glacier or ice stream: determining the mass balance, calculating the force budget and investigating relic features. Previous studies conducted on Whillans Ice Stream have focused on one of these three methods. This project is unique because all three methods are assessed simultaneously, giving a more complete picture of the dynamics of WIS.

Two velocity data sets are used to complete this analysis – those derived from photogrammetry, and those derived from interferometry. Repeat aerial photography was obtained for four sections of the ice stream in the 1985, 1986 and 1989 seasons. Velocities were derived from these photographs using manual feature tracking techniques. The velocities obtained in this manner were compared to velocities collected in 1997 from interferometry (InSAR).

## CHAPTER 3

### DATA COLLECTION

#### 3.0 Overview

To do a complete investigation of WIS, many data sets were utilized. Two remotely sensed velocity data sets were used: Synthetic Aperture Radar Interferometry (InSAR) from 1997 and photogrammetry from 1985-1989. To complete mass balance calculations, ice thickness information and accumulation rates were needed. The force budget required estimates for surface topography, which were derived from the OSUDEM. Finally, Radarsat imagery and Declassified Intelligence Satellite Photography (DISP) were used for geophysical and flow dynamic assessments.

#### 3.1 Insar Data

##### ***3.1.0 Overview***

Synthetic Aperture Radar Interferometry (InSAR) is a widely used technique for measuring ice sheet surface velocities. In conjunction with the 1997 Radarsat Antarctic Mapping Project (RAMP) that produced high-resolution images of the Antarctic continent, interferometric data was generated for selected areas, including the Ross Ice Streams (Forster et al., 1998). Previous velocity measurements of these ice streams were patchy at best. Ground based measurements only provide velocity measurements at a

specific point, and are precarious to collect. Velocities derived from photogrammetry are more dense, but the photoblocks still only cover a small portion of the ice stream. InSAR data however, provides closely spaced velocity measurements across much of the Ross Ice Streams. For the first time, the true pattern of velocities can be analyzed without relying on interpolation schemes to fill in areas without velocity data.

### ***3.1.1. Data Acquisition and Processing***

By analyzing the differences between coherently interfered pairs of complex SAR images, surface topography and motion can be measured. In this study, repeat pass interferometry was used as processed by Ian Joughin (1995).

The geometry of an interferometric SAR is shown in Figure 2, after Joughin (1995). Assuming a flat earth model where point P does not move during the two time-separated passes, point P has an elevation of  $z$ . The two satellite positions from sequential passes are denoted by  $S_1$  and  $S_2$ . During the first flight path, using satellite position  $S_1$ , the elevation is  $H$ . The distance from  $S_1$  to P is  $r_0$ . During the second flight path,  $S_2$ , the satellite has moved a distance  $B$  and is rotated by a tilt angle,  $\xi$ . The distance from  $S_2$  to the point of interest, P, is now  $r_0 + \Delta$ .

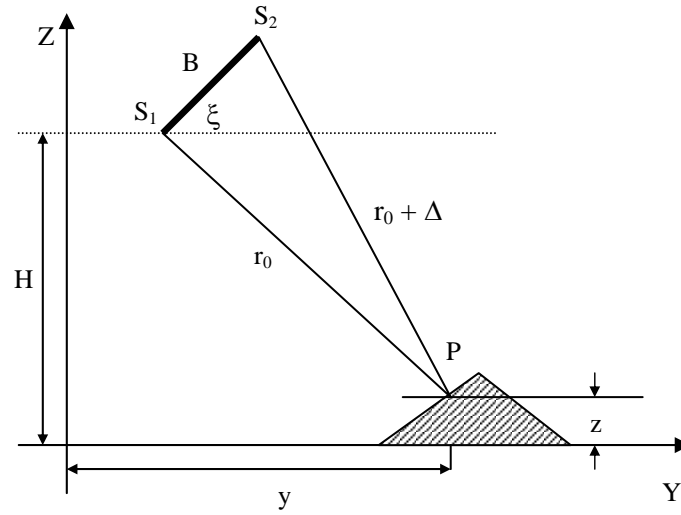


Figure 2. Geometry of cross-track interferometric SAR.

The range difference,  $\Delta$ , changes as a function of elevation change or surface motion between repeat passes. Motion displacements in the range direction can be expressed as changes in the  $y$  and  $z$  direction, using equation (2) (Joughin, 1995).

$$\Delta_{motion} = (y_2 - y_1)\sin\theta - (z_2 - z_1)\cos\theta \quad (2)$$

The steps involved in processing InSar data vary depending on the data that is available. Every application, however, includes some form of single complex image co-registration, interferogram formation, phase unwrapping, baseline refinement, and image geocoding (Zhao, 2001). This allows for a secondary approach, speckle matching, which yields

both components of the velocity vector. Velocity errors in the range direction of interferometry are 4 m/yr. Speckle matching errors are 20 m/yr in the range direction and 10 m/yr in the azimuth direction. For this study a total velocity error of 12 m/yr was applied.

Absolute control for InSAR data in this region was done using a select set of Transit measurements collected by Whillans (1993b). Since the photoblock velocities were tied to similar ground control points, a cyclical error was an initial concern. However, only poles in slow-flow zones were used for this technique (Joughin, pers. comm., 2002). Therefore, there should be minimal, if any, interference between InSAR and photoblock results.

Intricacies pertaining to the processing of InSAR data are beyond the scope of this paper. Interested readers can refer to Joughin (1995) and Zhao (2001).

### ***3.1.2 Application of InSAR data***

The magnitude of velocity was gridded in ArcINFO at a 50 m spacing interval and imported into ERDAS Imagine, a computer image processing software package. The contoured velocities are shown in Figure 3, with flowlines overlain on top. Velocity profiles along each gate were drawn. Only the component of velocity orthogonal to the gate was used in the mass balance calculation.

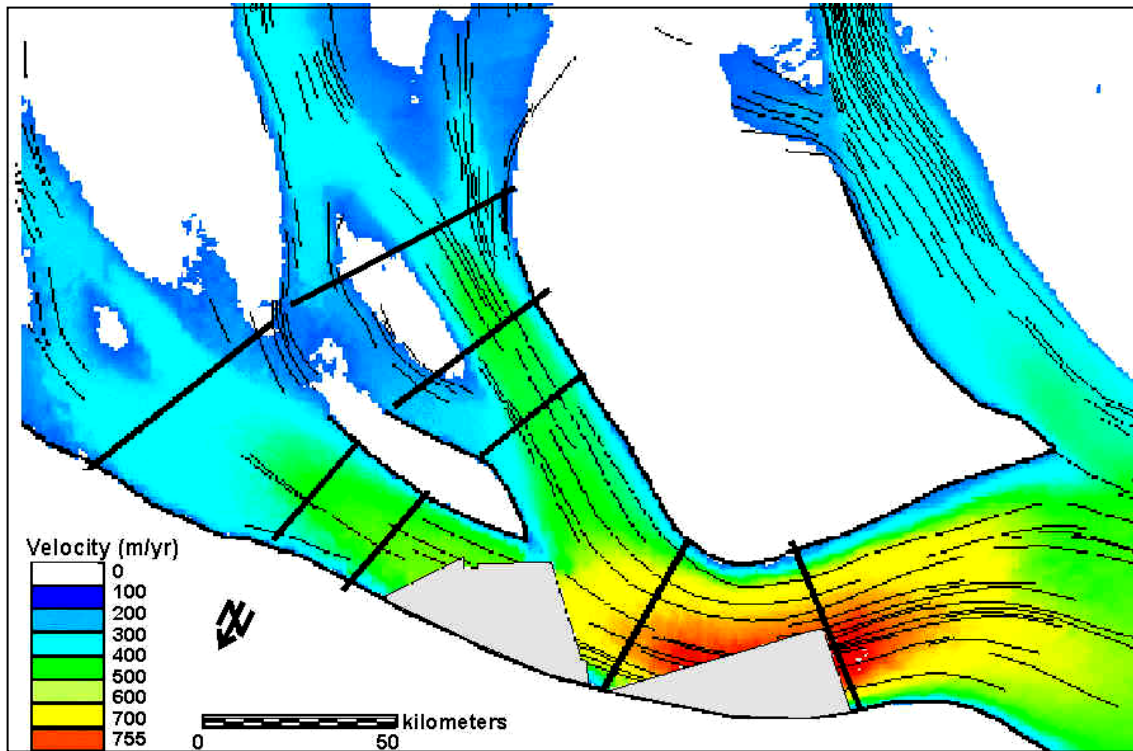


Figure 3: InSAR velocities for Whillans Ice Stream. Velocities under 50 m/yr are white and areas with no data are shaded gray. Thick black lines spanning across the ice stream represent flux gates used in the mass balance calculation. Thin black lines trending down the ice stream represent flowlines.

### 3.2 Photoblock Data

#### **3.2.0 Overview**

Repeat aerial photography was used to obtain closely spaced velocity measurements along Whillans Ice Stream. During the austral summers of 1985, 1986 and 1989, repeat images of six areas of Whillans Ice Stream were collected. The location of each image, or photoblock, is shown in Figure 4.

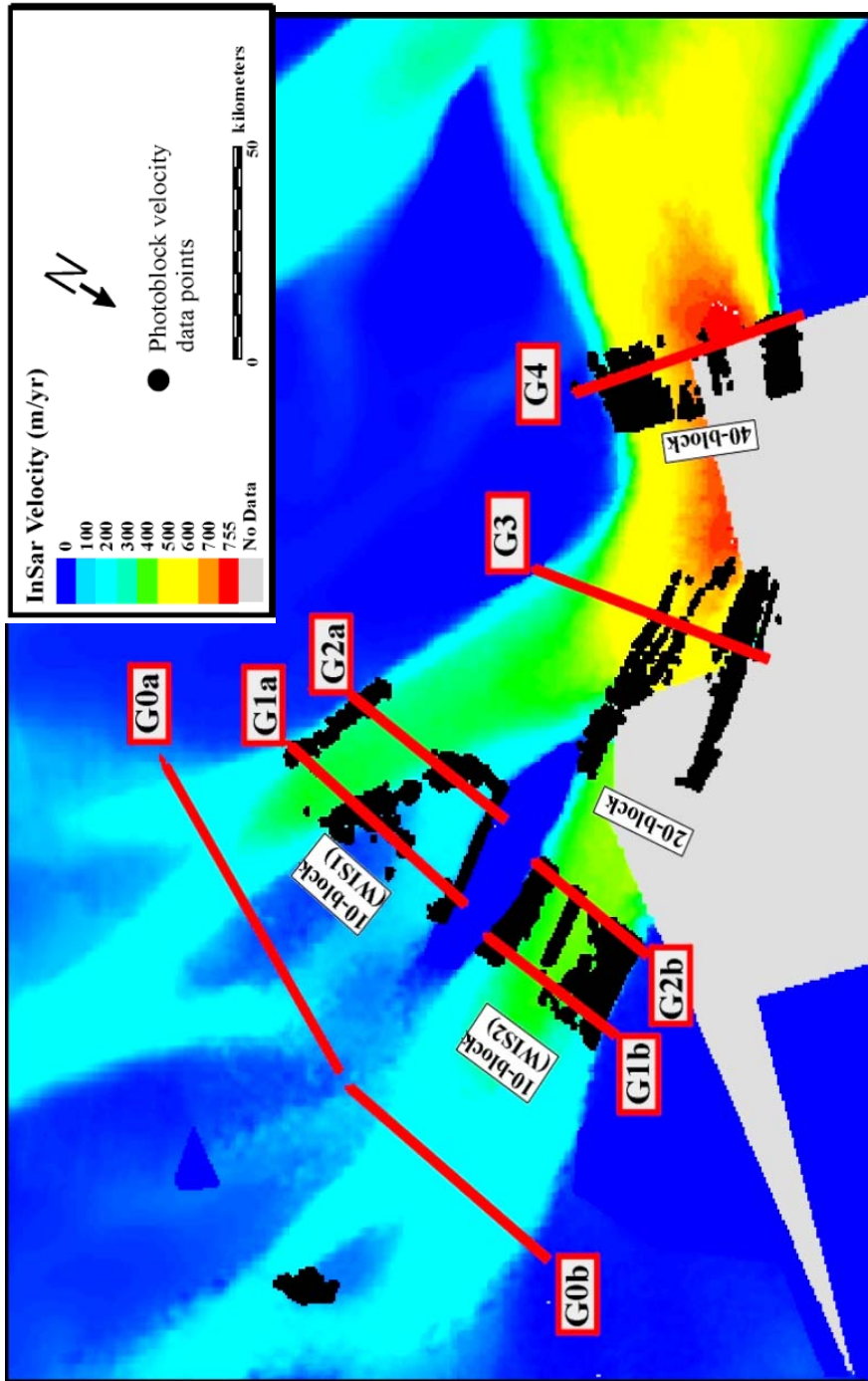


Figure 4: InSAR velocity field (background image) with the gray areas denoting no data zones. The locations of the velocity data points are shown as black dots.

Aerial photographs for the '10b2-block' and the '40-block' were collected in 1985 and 1986. Photographs for the '10b1-block' and the '20-block' were obtained in 1986 and again in 1989. Throughout this paper, an average date of 1986 is given to the photoblock velocities (unless the time-frame of each photoblock needs to be considered individually). Manual feature tracking, usually of crevasses, was performed for each location by Whillans, Tseng (1993c) and Jackson (1991).

### ***3.2.1 Data Acquisition***

Precise ground control points must be located before aerial photographs can be taken. Since there is no exposed bedrock adjacent to Whillans Ice Stream, ground control was established on the moving ice sheet. Slow-moving Transit stations set up by Whillans in 1984-1985 were used as ground control points and as corner points for the photoblocks (1987). Black plastic sheets, 3 m by 3 m, were attached to bamboo poles and suspended several decimeters above the surface to avoid snowdrift. These sheets were easy to locate on the images, thus simplifying the coregistration process (Whillans and Bindshadler, 1988).

The aerial photographs are tied to two types of ground control stations – those on ridge ice, and those on the fast moving ice stream. The velocities of these stations were first determined by point-positioning with precise satellite orbits from the U.S Defense Mapping Agency (Whillans 1987). To geometrically correct the aerial photography, Transit (or Doppler) satellites were tracked at each station. All ground control points were revisited and resurveyed for approximately 24 hours at each photograph epoch. The station positions were then processed together with orbital information to precisely

identify their location. Finally, all simultaneously operating receivers were tied to two slow moving sites located on the ridge ice. This method of network adjustment improves the precision of the fast-moving stations (Whillans et al., 1993; McDonald and Whillans, 1988, 1992).

The photographs were collected with a Wild RC8 camera in a LC-130 Hercules or Twin Otter airplane. The altitude at which each photoblock was taken varied, but was in the range of 6000-8000m., transforming into a map scale of 1:50,000. Great care was taken to collect the photographs at similar sun-illumination angles and scales and to obtain end-lap coverage of ~60% and side-lap coverage of 20% (Whillans et al., 1993c).

### ***3.2.2 Data Processing***

A block adjustment aerotriangulation calculation was applied to form a mathematical photo-mosaic that was tied to ground control points for each epoch (Whillans et al., 1993c). Distinctive features on crevasses and drift mounds were then tracked in sequential images. The distribution of data therefore is irregular throughout the block and absent in the crevasse-free center of the ice stream. Whillans, Tseng and Jackson derived the velocity components from the aerial photographs (1991, 1993c).

At the start of this project, the only processing that was needed involved transforming the velocity information from a local coordinate system to a WGS84 geographic one. The origin and rotation of each photoblock's local coordinate system is listed in Appendix A. Once in geographic coordinates, the velocity data points were entered into ArcINFO with no interpolation and imported into Imagine.

Photoblock velocities are derived from feature tracking and are obviously dependant on the presence of features. Especially in the center of the ice stream, these features are absent. Therefore, the velocity profiles along each transect are not always complete. A cubic spline of the measured velocities filled in the gaps.

### ***3.2.3 Photoblock Accuracy***

Errors associated with the photoblock velocities can originate from the ground control points, photograph measurements, or coordinate transformation. The relative errors in ground control are 0.4 m/yr and are systematic within a portion of the photograph. Errors associated with feature tracking techniques between epochs add up to 1.7 m/yr and should be random. Distortions on the photoblock due to weak ground control ties are 2.1 m/yr and are most likely systematic over the area of the photograph. Whillans (1993c) uses a total velocity uncertainty of 3.2 m/yr.

To eliminate errors associated with the absolute location of the photoblocks, cross-correlation estimates of photoblock velocities and InSAR velocities were conducted across numerous transects. In one case, for the 10-block on WIS2, the cross correlation result indicated an error in geolocation by 2 km (refer to Figure 4 for the photoblock location). The block was then shifted to the south by that amount. Figure 5a shows the InSar velocity profile and the interpolated photoblock velocity profile for transect G2a, after the block was corrected.

Figure 5b shows the results of the final cross-correlation test between the photoblock and InSar velocity data points. A correlation value of 1 at no lag distance indicates a good correlation between the two data sets. The results for the other blocks showed similarly good correlations between the two data sets. As a result, a total error of 4 m/yr was assigned to photoblock velocities.

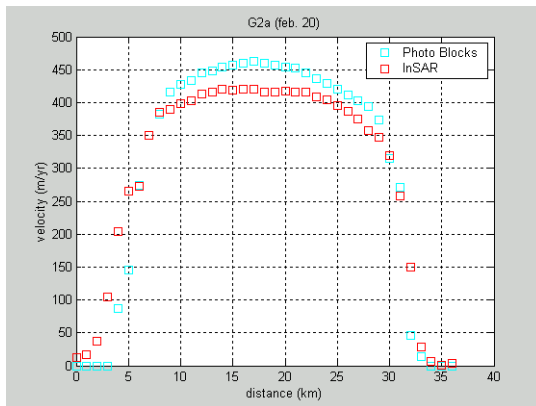


Figure 5a

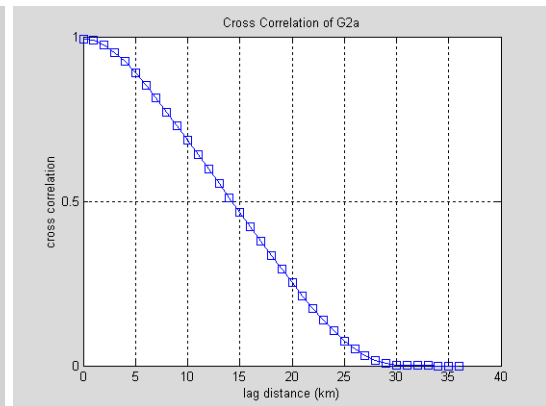


Figure 5b

Figure 5: Cross-correlation of the InSar and photoblock data sets. a). An overlay of the two velocities (InSar and Photoblock) along transect G2a. b). Cross-correlation result for the two velocity profiles in 5a.

### 3.3 Radarsat Imagery

#### **3.3.0 Overview**

The first, high-resolution synthetic aperture radar image data set over Antarctica was taken using the Canadian Radarsat-1 satellite in autumn of 1997. It only took 18 days to obtain a nearly instantaneous picture of Antarctica, composed of over 3000 frames (Jezek et al., 1998b). The improved, radiometrically calibrated and geometrically accurate mosaic of Whillans Ice Stream is shown in Figure 6.

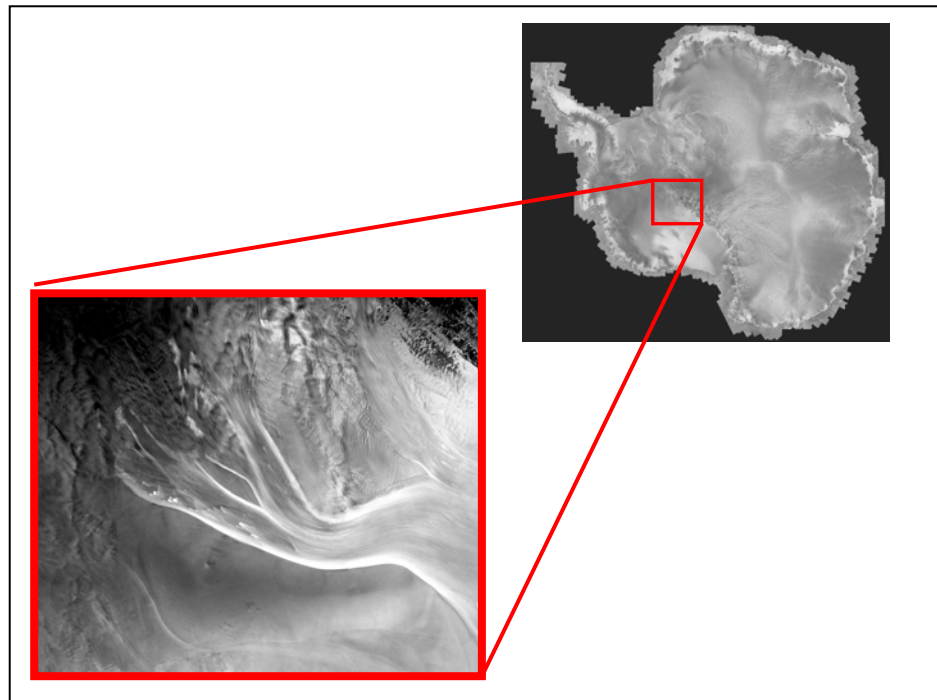


Figure 6: Radarsat mosaic of Antarctica and the location of Whillans Ice Stream

### ***3.3.1 Data Processing***

Processing and calibrating of the Radarsat-1 mosaic was done at The Byrd Polar Research Center, the details of which can be found in various papers (Forster et al., 1998; Jezek et al, 1996, 1999, 1998a; Jezek et al., 1998b; Mahmood et al., 1998). For this project, the Radarsat image of Whillans Ice Stream was used predominantly for feature tracking purposes. The relationship between shear margins, surface features, flowlines and velocity patterns were investigated. These features were also compared to similar features recognizable in the DISP imagery from 1963. Directional filters were applied to enhance certain features, especially those transferred from the bed and flowlines.

## **3.4 Declassified Intelligence Satellite Photography**

### ***3.4.0 Overview***

For security reasons during the Cold War, the U.S. launched three early reconnaissance satellites to image the Earth's surface. These satellites - under the code names Corona, Argon and Lanyard - operated from August 1960 to May 1972, collecting data in utmost secrecy (McDonald, 1995). In 1995 President Clinton ordered declassification of these historic satellite images for scientific use. In Antarctica, Declassified Intelligence Satellite Photography (DISP) has been used extensively to document changes that have occurred since 1963 (Jezek, 1998; Bindschadler and Vornberger, 1998; Kim, 1999).

The Argon program was the only satellite that collected imagery of Antarctica. This mission was primarily cartographic, collecting black and white film at a nominal scale of 1:4,250,000 (Bindschadler and Seider, 1998). The resolution ranges from 2-140 m and single frame camera coverage was 540 km by 540 km. Table 1 lists the spatial and temporal characteristics of the ARGON DISP imagery.

<b>System</b>	<b>Argon Satellite</b>
Camera Type	Frame
Film Format (mm)	120 x 120
Focal Length (mm)	76
Resolution of Film (lp/mm)	30
Ground Resolution (m)	138
Nominal Altitude (km)	313.2
Ground Coverage (km)	540 x 540
Period of Operation	1961 – 1964
Photo Scale on Film	1:4,250,000

Table 1: Characteristics of Argon (McDonald, 1995)

### ***3.4.1 Data Processing***

Kim (1999) orthorectified and calibrated the DISP imagery used in this project. First, distortions due to the camera lens, atmospheric refraction and Earth curvature were removed (Lillesand and Keifer, 2000). Next, differential rectification, which corrects for terrain displacement, was conducted using a digital elevation model (DEM) of the area.

In conjunction with the Radarsat Antarctic Mapping Mission (RAMP) in 1999, a high-resolution DEM was produced. The imagery was translated to ground coordinates using collinearity equations (Kim, 1999). Figure 7 shows the four DISP images used to cover Whillans Ice Stream in 1963. The tie points and ground control points that were used to register the images are also shown. The error associated with the ARGON imagery is 140 m (Kim, 1999). Once the final image was acquired for this project, minimal data processing was done. Directional filters were used to bring out specific surface features (flowlines, bed features, crevasse patterns) that are hard to see on the original image.

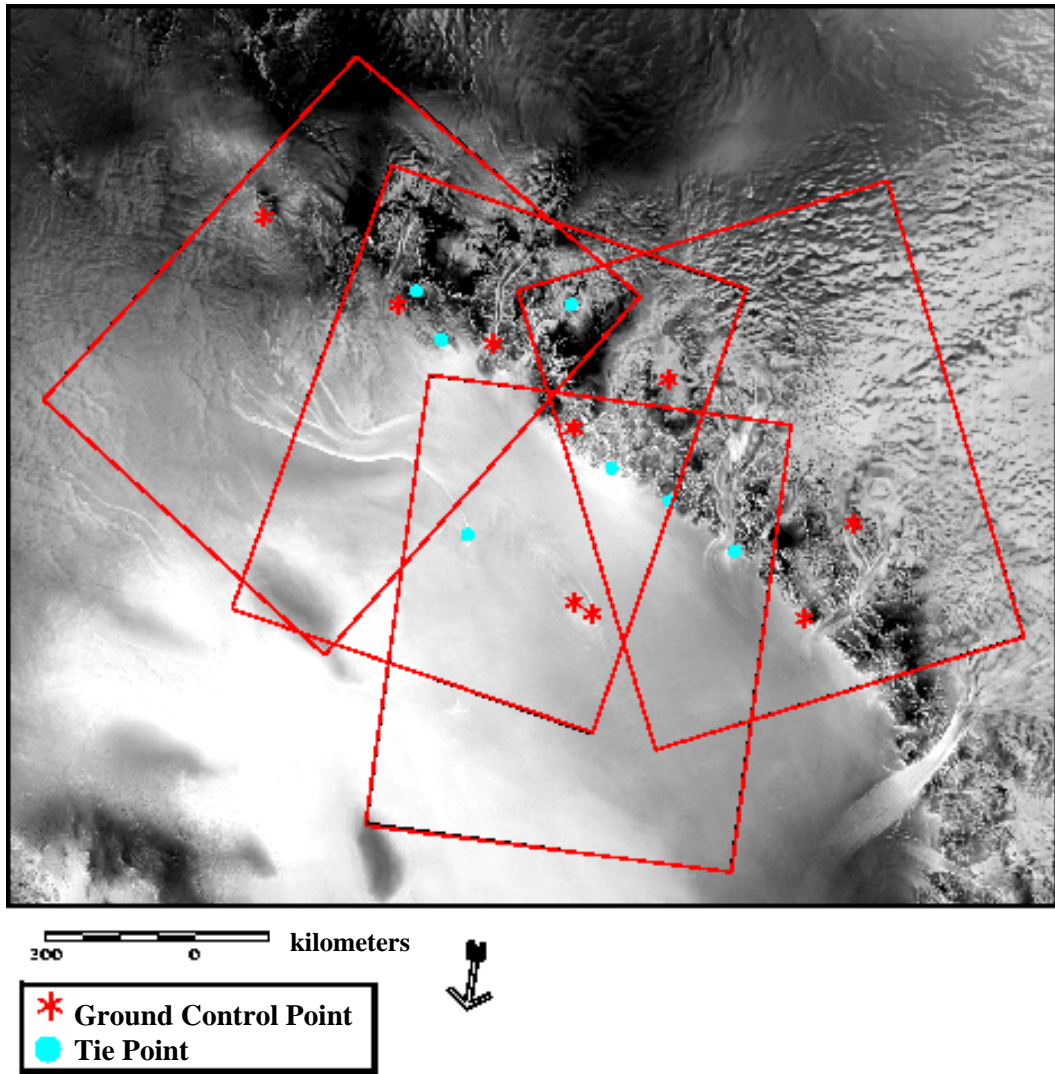


Figure 7: The outline of the DISP images used for coverage of Whillans Ice Stream. The location of the tie points and ground control points used to register the DISP images are shown as well.

### 3.5 Bed Topography (BEDMAP)

In 1984-1985, Shabtaie et al. (1987b) conducted airborne radar soundings of the ice sheet surface. The mapping used a combination of airborne radar sounding and ground-based surveying for control points. Each sounding flight line was tied to several ground control stations to improve accuracy. The bed topography used in this study was compiled and collected by BEDMAP, a product of the British Antarctic Survey (Lythe and Vaughan, 2000). The data, gridded at 5 km intervals, was obtained from BEDMAP and imported into ERDAS Imagine for analysis. An error of 25 meters was used for the bed topography. The ice-thickness was derived from the same technique. An error of 18 meters was used, as suggested by Whillans (1988). Figure 8, is a 3-D image of the bed topography surrounding Whillans Ice Stream.

### 3.6 Surface Topography (OSUDEM)

A number of different topographical data sets of Antarctica were integrated to produce a single high-resolution DEM. Ground-based data sets, satellite radar altimeter data and airborne radar data were all incorporated into a single GIS environment (Liu et al. 1999). Specifics of this project are described by Liu (1999). The DEM has a 200 meter post spacing that is derived by resampling and interpolation. On the Antarctic Peninsula and the Transantarctic Mountains, the resolution is 200m. At the coast it is 400m. In the interior it is 5 km. The vertical accuracy for the Ross Ice Streams is 15 m (Liu et al., 1999b). A 3-D image of this DEM over the Whillans Ice Stream is shown in Figure 8.

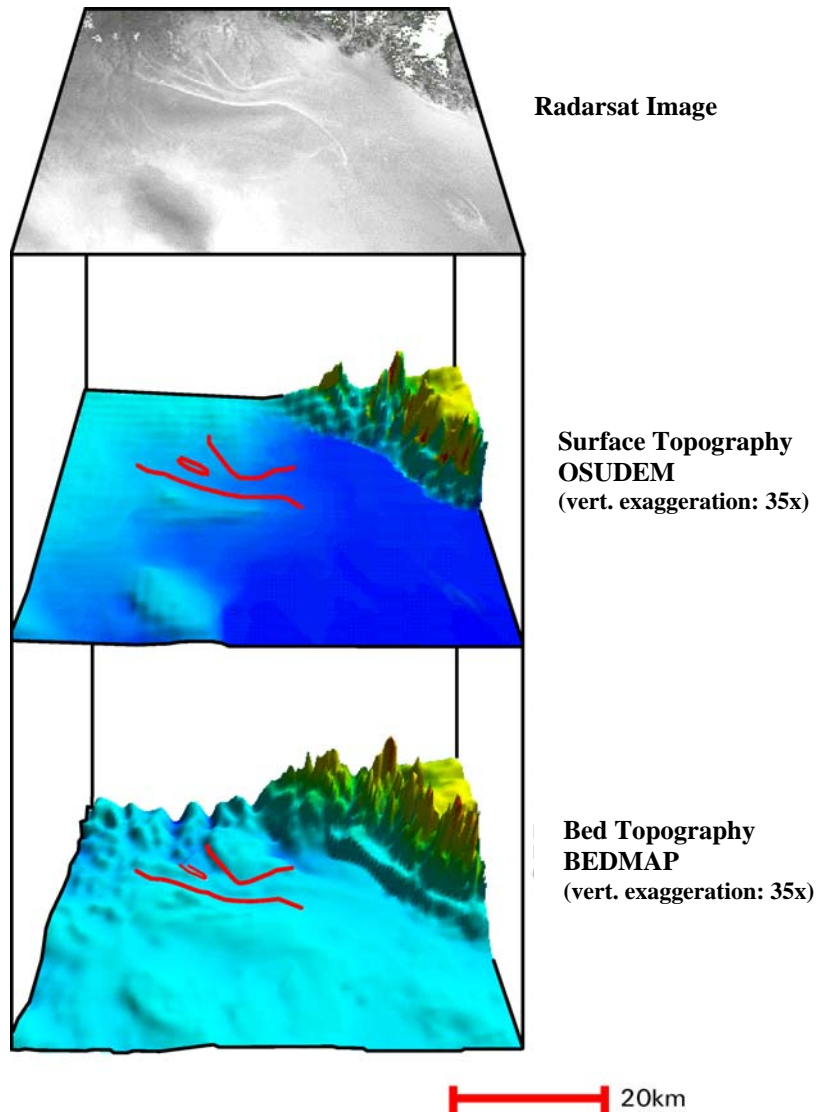


Figure 8: Radarsat image, Surface DEM and Bedrock Topography of Whillans Ice Stream.

### 3.7 Accumulation Rates

Accumulation rates published for WIS by Venteris and Whillans (1998) were used for this study. They analyzed 70 shallow firn cores throughout the Ross Ice Streams and modeled the variability in accumulation rates. The published rates have associated errors of ~15% or 0.016 m/yr ice equivalent. The spatial variability of accumulation rate is most important for mass balance investigations that include the catchment area. For the purposes of this study, a range of accumulation rates from 13 cm/yr at the upstream end (gates G0), to 11 cm/yr at the terminus (gates G3 and G4) were used. The errors are significantly small and do not affect the final flux results.

### 3.8 Compilation of data sets

When all the information listed above is combined, a complete analysis of Whillans Ice Stream is possible. A composite of these data sets is shown in Figure 8, which portrays the bed topography and surface topography that defines Whillans Ice Stream. Two aspects of this image are worth noting. First, tributary WIS1 (the northern tributary) appears to be more topographically confined than WIS2 (the southern tributary). Second, WIS1 is significantly thicker with a steeper (slightly) surface slope.

Common transects were drawn across the gridded velocities derived from InSAR and Photogrammetry. Transects were limited by the location of the photoblocks, as was shown in Figure 4.

Whillans Ice Stream has a complicated flow pattern since it is comprised of numerous intersecting tributaries. Most flowlines have a significant degree of curvature and, as a result, transects are not always orthogonal to them. To correct for this, the vector product relative to the angle between the velocity vector and the surface normal is taken when computing the final velocities. Graphs of InSAR and photoblock velocities and bed topography are shown for each gate in Figures 9a-c.

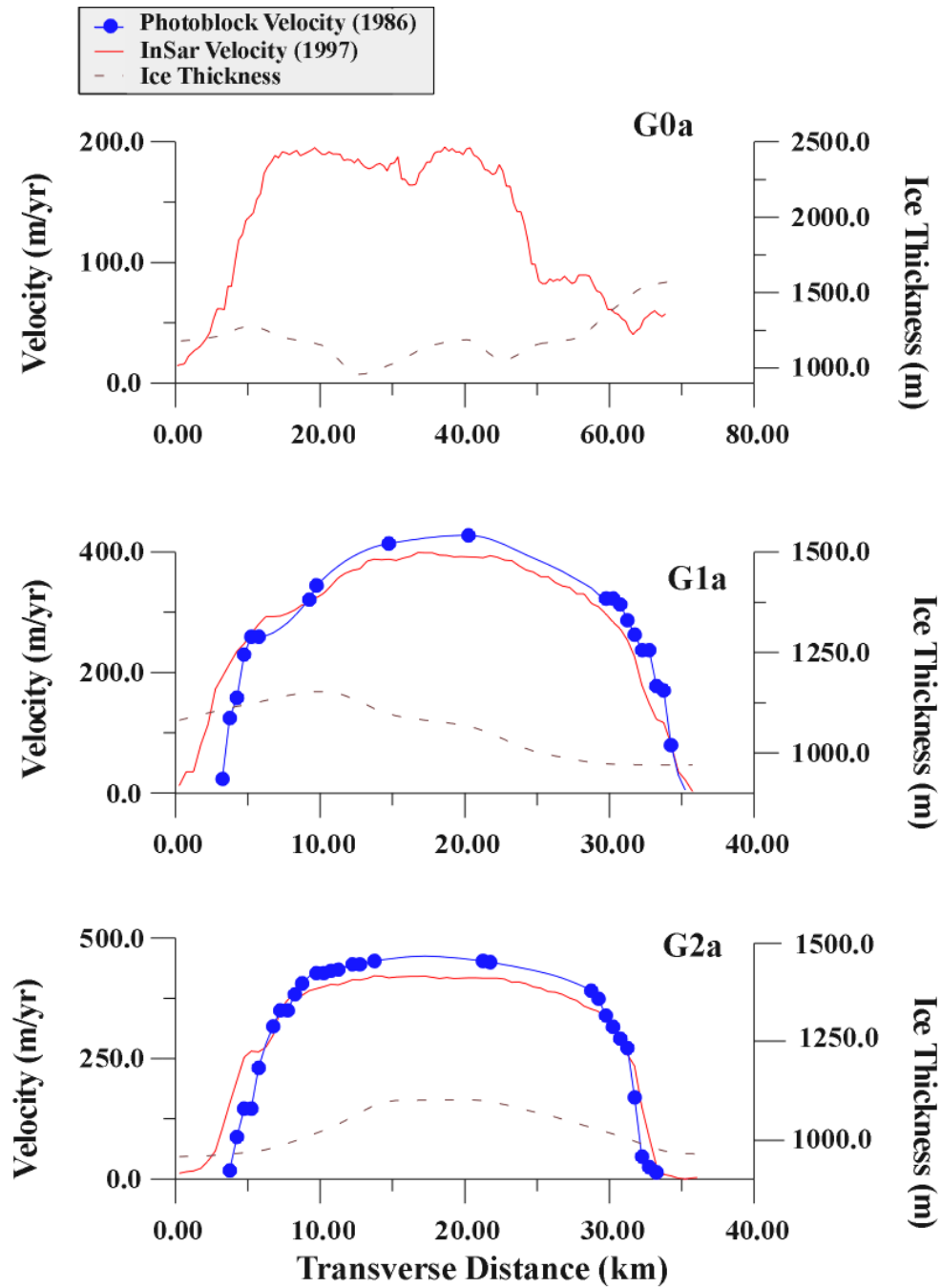


Figure 9a: Velocity profiles along WIS2 (transects G0a-G2a). The solid red lines represent InSAR velocities. The blue dots represent measured photoblock data points; the line connecting them is interpolated. Both velocities refer to the left-and y-axis. The dashed black line is ice thickness, represented by the y-axis on the right.

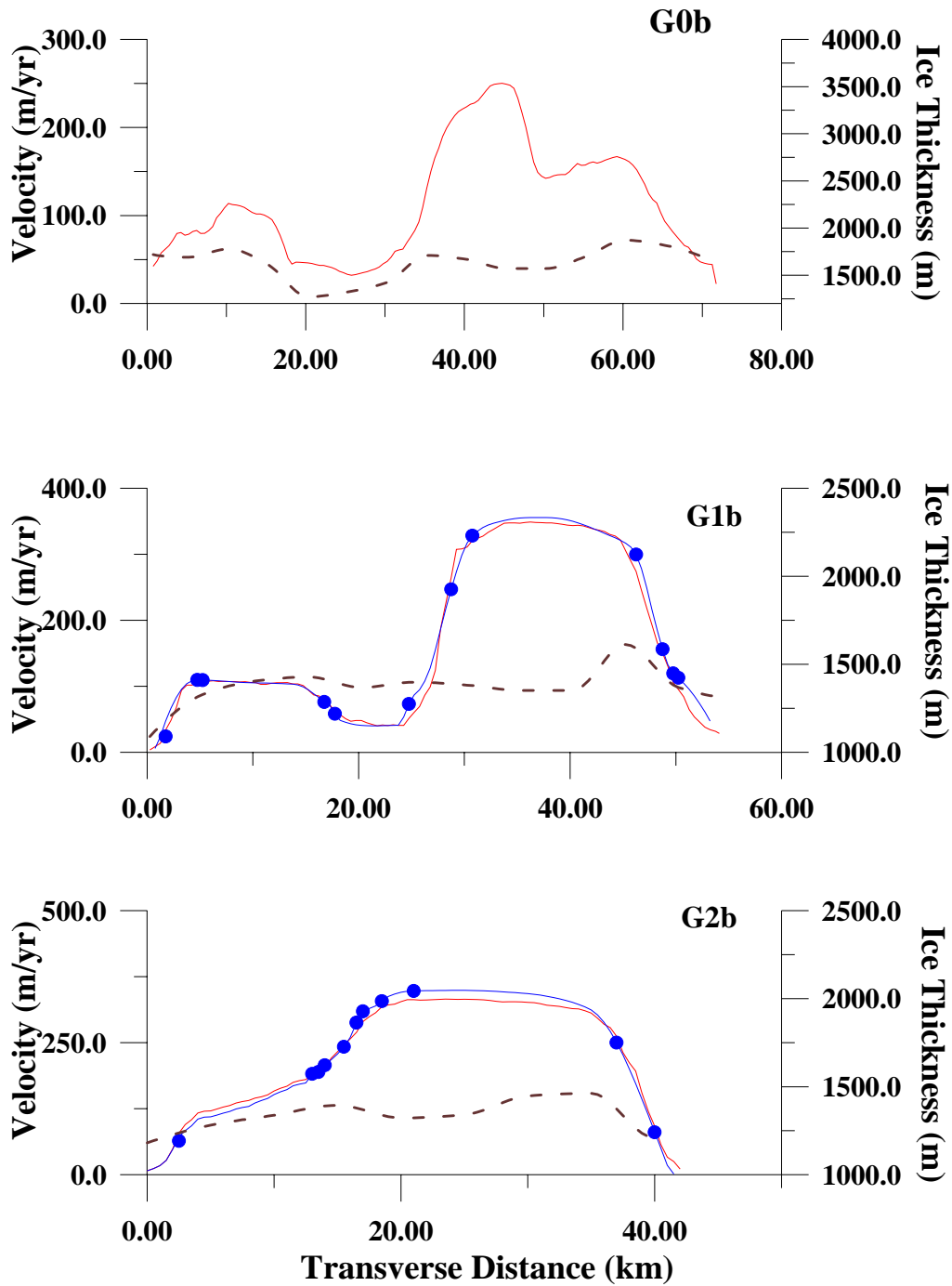


Figure 9b: Velocity profiles along WIS1 (transects G0b-G2b). The solid red lines represent InSAR velocities. The blue dots represent measured photoblock data points; the line connecting them is interpolated. Both velocities refer to the left-and y-axis. The dashed black line is ice thickness, represented by the y-axis on the right.

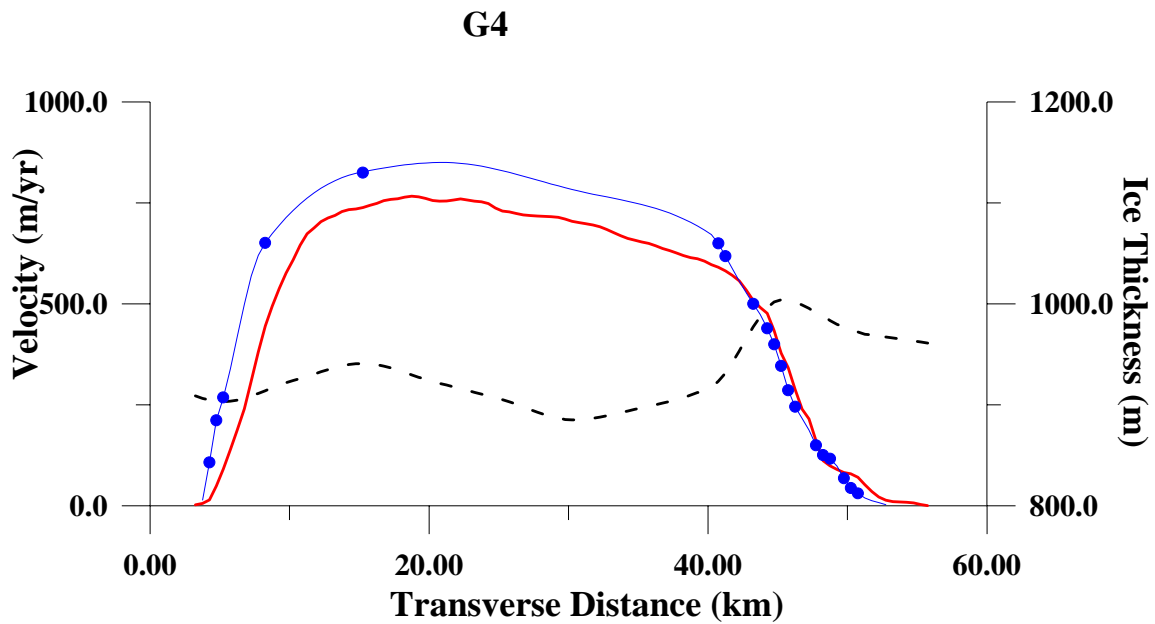
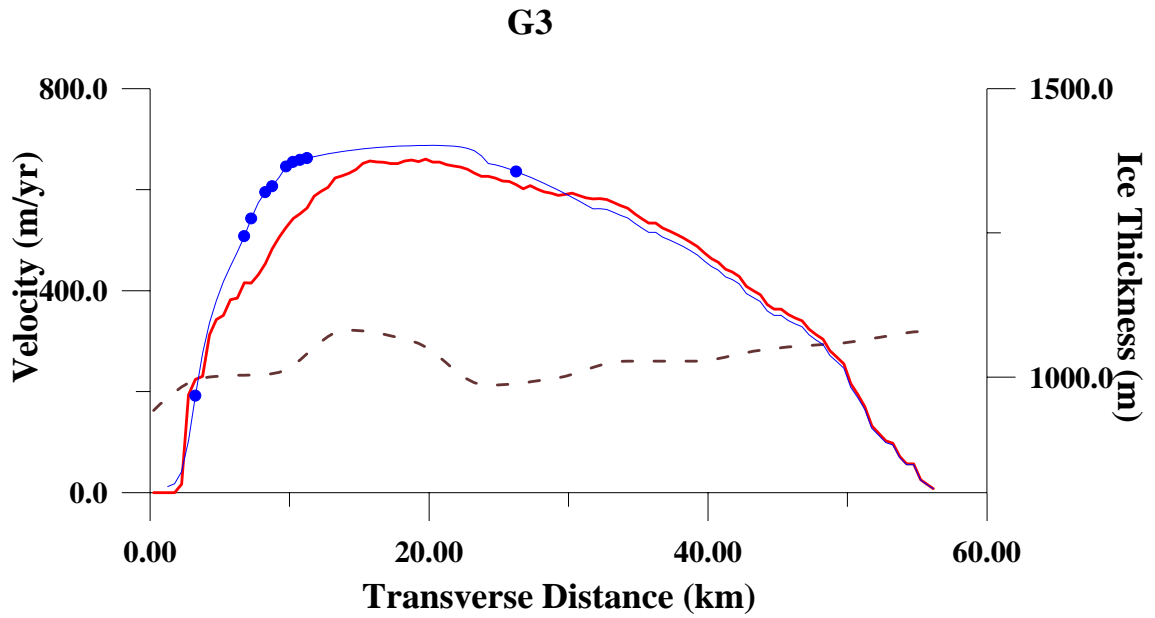


Figure 9c: Velocity profiles along WIS (transects G3-G4). The solid red lines represent InSAR velocities. The blue dots represent measured photoblock data points; the line connecting them is interpolated. Both velocities refer to the left- and y-axis. The dashed black line is ice thickness, represented by the y-axis on the right.

## CHAPTER 4

### SPATIAL AND TEMPORAL CHANGES IN FLOW DYNAMICS

#### 4.1 Introduction

Transects that intersect both the photoblock and InSAR data sets were used to analyze spatial and temporal changes of the ice stream. In particular, velocity fields, strain rates, and shear stresses are assessed. By overlaying these results onto a Radarsat image, a unique investigation of surface features and their relationship to flow dynamics can be made.

#### 4.2 Velocity Variations

##### ***4.2.1 Spatial Variations in Velocity***

Spatial variations in velocity are determined by assessing the velocity profiles along each transect (Figure 10). At the catchment there is a visible effect of merging tributaries. The velocity profiles for G0a and G0b are not parabolic and smooth, but rough and variable. At G0a, the majority of the ice comes from a tributary to the north. Surprisingly, the two linear flow stripes (indicated by the green arrows) have only a subtle signature in the velocity profile.

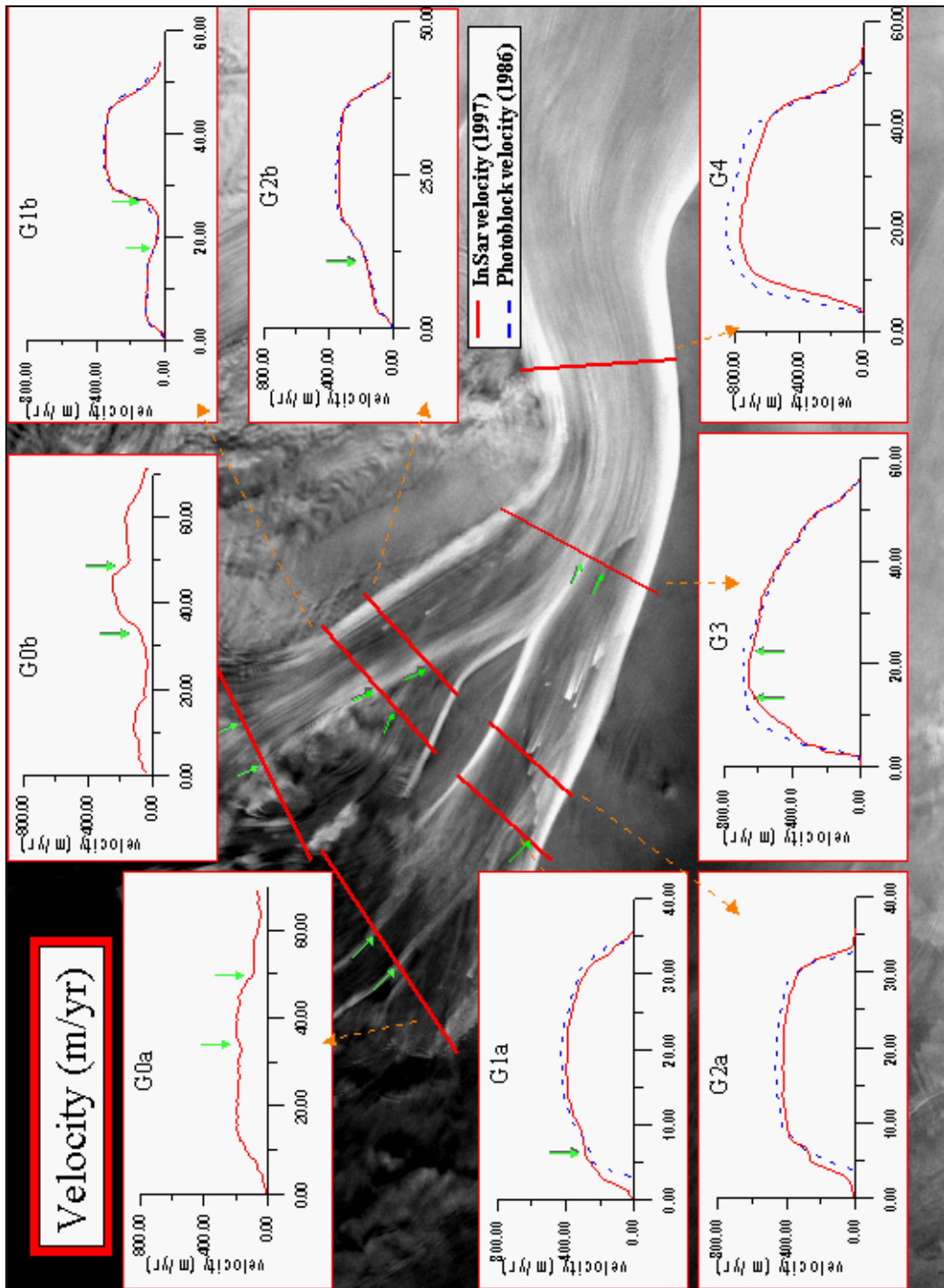


Figure 10: Spatial and temporal changes in velocity along Whillans Ice Stream. The solid (green) arrows are pointing to features noticeable on the Radsat imagery and their translation onto the velocity profile.

In contrast, the tributaries at gate G0b have a more pronounced effect on the velocity profile. The fastest ice comes straight down the center, in between the two green arrows. Adjacent to these arrows (on both sides) are smaller tributaries feeding into the trunk of WIS1. The northern tributary is separated by a bedrock feature over which there is minimal flow. In comparing these two catchment areas it is even more surprising that the linear crevasse features in G0a do significantly affect the velocity profile. This observation implies that these features are relic margins that no longer sustain high strain rates.

Along the northern part of Whillans Ice Stream (WIS2) the velocity profiles are very symmetric about the centerline (transects G1a and G2a). Across G1a, a bedrock feature causes a slight dip in the otherwise perfectly parabolic velocity profile (a green arrow points to this feature on both the imagery and the velocity profile). In 1986, the shear margin was located just north of this bedrock feature. In 1997, the shear margin is approximately 3 km north of the bedrock feature.

The velocity profiles along WIS1 illustrate how a merging tributary is incorporated into the main trunk. At G1b there are two distinct flow structures, separated by an area where there is no flow (in between the two green arrows). Downstream at G2b these two tributaries have merged (at the arrow), but the velocity profile is still not smooth. Since there was a significant velocity contrast between the two tributaries, the northern half of WIS1 is still slower.

There is no signature of WIS1 and WIS2 merging in the velocity profile at G3. The second arrow along this profile indicates where the two tributaries merge. The smoothness of this profile is unlike G2b, which shows the boundary of the northern

tributary as it coalesces with WIS1. G3 has a smooth profile, albeit asymmetric, because WIS2 and WIS1 both maintain similar velocities of 400 m/yr. The asymmetry is probably due to WIS2 being squeezed as it merges with WIS1. This asymmetry is less noticeable downstream at G4. The first arrow along the G3 profile points out a possible bed feature expression. Velocities are slightly depressed just up-stream of a feature that is very noticeable on the Radarsat imagery.

#### ***4.2.2 Temporal Variations in Velocity and Flow Dynamics***

Temporal variations in velocity are assessed by comparing time sequential data sets. The first comparison is between photoblock velocities from 1986 and InSar velocities from 1997. A second, more qualitative comparison of changes in flow is made between the DISP imagery and Radarsat imagery.

##### ***4.2.2.1 Velocity Variations***

Unfortunately, the lack of photoblock data in the catchment area prohibits comparisons there. Changes along WIS2 between 1986 and 1997 show a decrease in velocity of ~50 m/yr and a widening of the margins, especially to the north. This is most likely due to the smooth bed topography that is only on the northern edge of WIS2, making migrations more feasible. WIS1 is tightly bound by bed topography and therefore, exhibits only slight changes at the margins accompanied by a small deceleration. G3 and G4 show a significant degree of deceleration over the past decade, especially at the northern edge.

The deceleration at G4 is associated with an inward migration of the northern margin. As the ice stream decelerates the strain rate at the margins decreases and the surrounding ice gets colder until it is no longer actively deforming. This process causes the inward migration of the shear margin.

The southern half of the G3 velocity profile (after the second arrow) was purely interpolated, since the photoblock only extended halfway across the ice stream. Since the southern margins of G2a, G2b and G4 all exhibit little change, it seemed appropriate to simply overlay the two profiles.

#### ***4.2.2.2 Flow Direction Variations***

Comparing 1963 DISP imagery with 1997 Radarsat-1 imagery allows for a qualitative assessment of changes in flow features. In particular, directional features such as flowlines and shear margins were compared. Because some of these features were difficult to locate on the original image (especially the DISP imagery), directional filters were applied. To enhance flowlines and shear margins that trend east-west, north-south Prewitt filters were used. Vector layers were drawn on each image, tracing the flowline orientation. A useful tool in comparing the flowlines in both images is to overlay the time-sequential vector layers. The results are shown in Figure 11. It should be noted that this is not a feature-tracking technique, since the vector layers are not representing a displacement of a specific feature. Instead, the orientation of flow in that area is outlined. The most change is occurring along WIS1, the southern tributary. The 1963 flowlines (blue) converge more down-flow, especially adjacent to the tip of the unicorn (the stagnant feature dividing WIS1 and WIS2). As the two tributaries coalesce, WIS1 is

squeezed significantly, narrowing as it combines with WIS2. WIS2, on the other hand, does not appear to change width when it combines with WIS1. This observation implies that WIS2 is the ‘dominant’ tributary in 1963.

In 1997, however, the roles reverse. The red flowlines (Figure 11) indicate that WIS2 narrows dramatically as the two tributaries merge. In addition, the flowlines on WIS1 are straighter throughout its length and are not converging downflow.

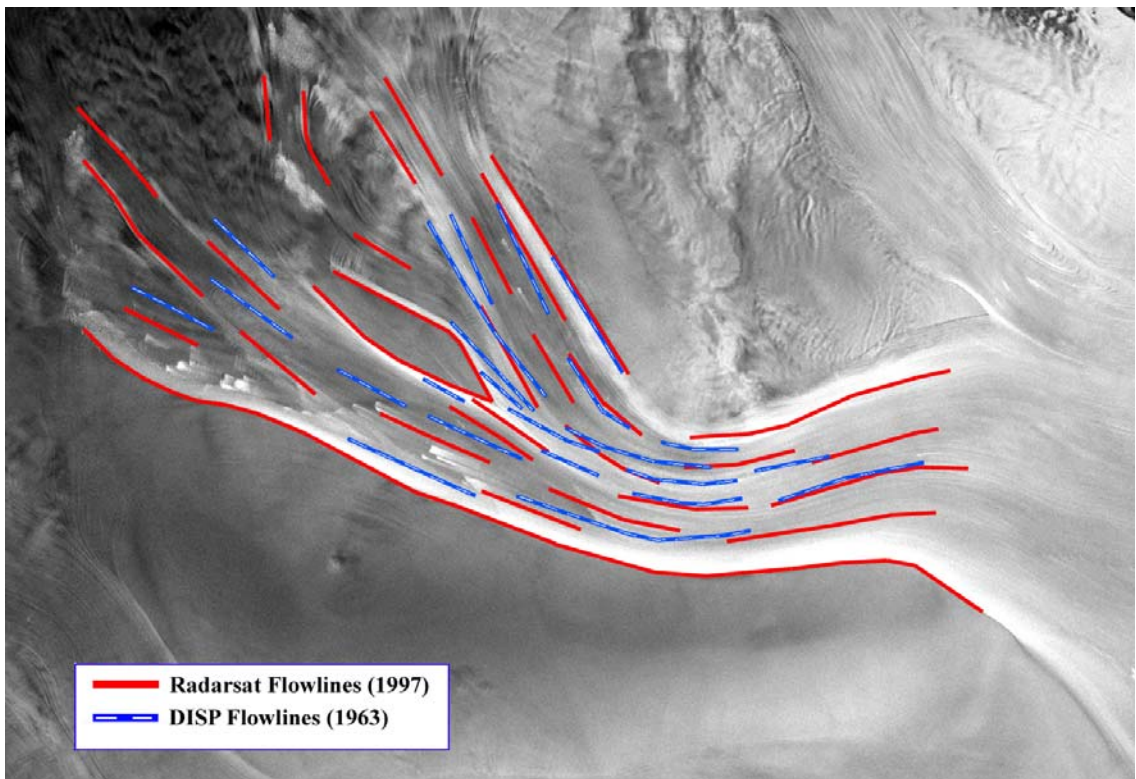


Figure 11: Comparison of DISP (blue) and Radarsat flowlines (red) overlain on a Radarsat image of Whillans Ice Stream.

Margin migrations are difficult to detect when comparing these two images because the shift is small and within the error limits associated with comparing two very different images. The margins are very noticeable on the Radarsat imagery, but very broad as well. Difficulty arose when outlining these margins because there is a very bright white region followed by a sharp contrast to black. This effect is due to the inherent differences between DISP and Radarsat imaging techniques. The north face of every feature is illuminated and the south-facing side is experiencing a shadow effect. To maintain consistency when tracing these features, the outer boundary of the white region of the feature was traced.

Even though a directional filter enhanced several features in the DISP imagery, the resolution was still much coarser than in the Radarsat image. In this imagery, the south-facing sides of features were more noticeable than the north-facing ones. Errors arise when comparing the location of features (as opposed to the orientation) because of the inherent differences in the imagery produced by these two satellites.

#### 4.3 Shear Strain Rate Variations

The shear strain rate is mainly determined by the transverse gradient in the along-flow velocity  $dU_x/dY$ . Previous studies indicate that gradients in longitudinal strain are negligible (Whillans and Van der Veen, 1993b) and are therefore ignored in this analysis. Strain rates are calculated from the velocity profiles at each transect for InSAR and photoblock data sets (Figure 12).

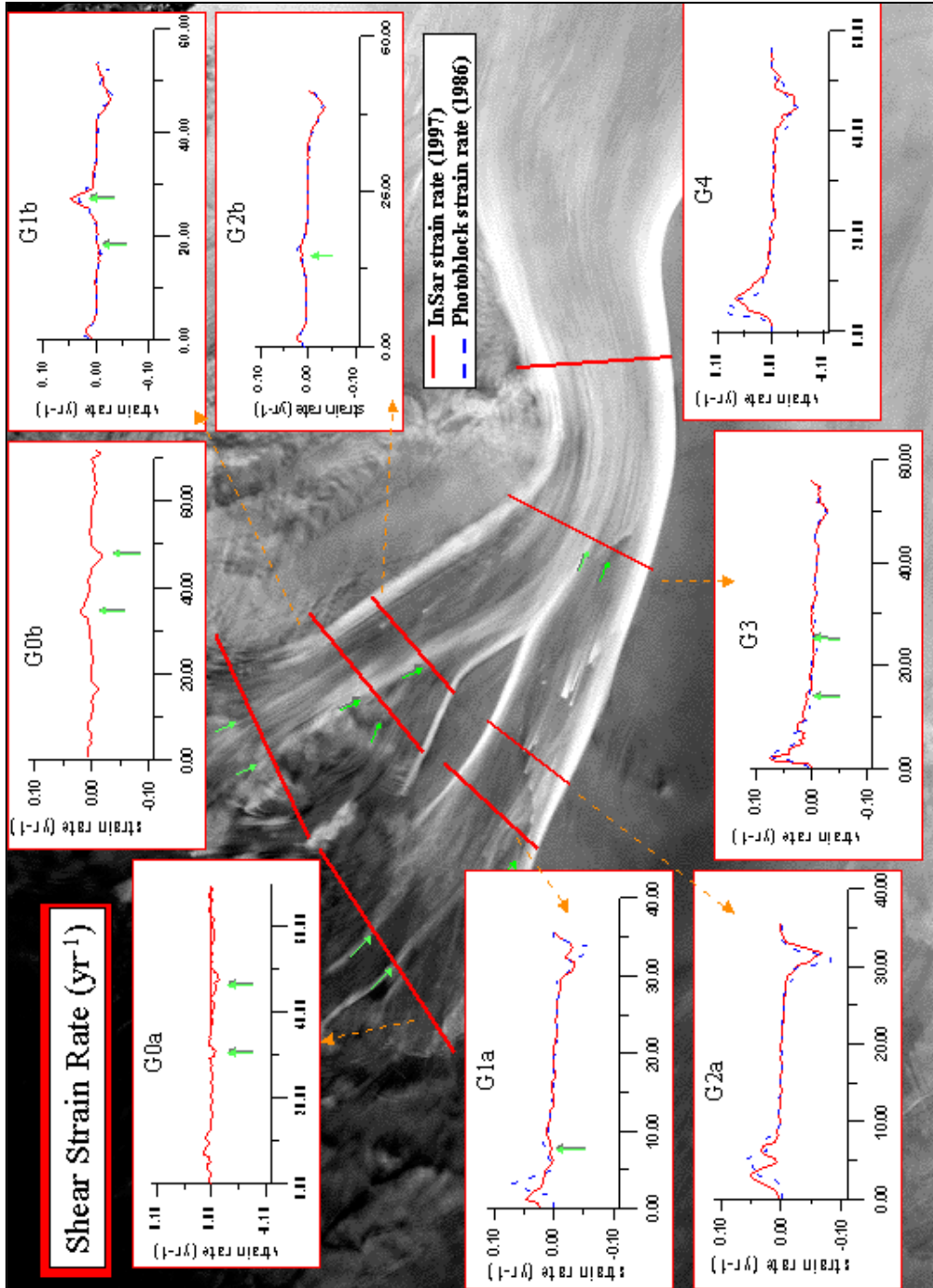


Figure 12: Shear strain rate variations across Whillans Ice Stream. Dashed (blue) lines represent Photoblock results, solid (red) lines represent InSAR results.

### ***4.3.1 Spatial Variations in Shear Strain Rate***

At the catchment, shear strain rates are very small (Figure 12). The linear flow features noticed at the G0a transect barely show up on the strain rate profile, with strain rates ranging from 0.00 to  $\pm 0.01 \text{ yr}^{-1}$ . This adds credence to the previous suggestion that these are relic features. In comparison, the strain rate is twice as large for the tributaries in G0b, which do not show crevassing.

The shear strain rates across WIS1 and WIS2 are significantly different. The most noticeable aspect of the WIS2 strain rates is that they are almost perfectly flat at  $0.00 \text{ yr}^{-1}$  at the center of the ice stream. At the margins the strain rates peak at  $\pm 0.08 \text{ yr}^{-1}$ . WIS1 sustains much lower strain rates at its shear margins than WIS2. This is especially true at the northern margin of WIS1, which has a strain rate of less than  $\pm 0.02 \text{ yr}^{-1}$ .

The shear strain rate of G3 is very asymmetric. This is not surprising since the strain rates of WIS1 and WIS2 are very different. The north margin of G3 matches the north margin of G2a, with a strain rate of  $0.08 \text{ yr}^{-1}$ . Conversely, the south margin of G3 matches the south margin of G2b, with a strain rate of  $-0.02 \text{ yr}^{-1}$ . The surprising aspect of the G3 profile is that there is no strain rate signature where the two combine (at the second green arrow). Further down-flow, at G4, the asymmetry noted at G3 has diminished greatly. The northern margin still hosts a slightly larger strain rate, but not by much.

### 4.3.2 Temporal Variations in Shear Strain Rate

Temporal variations in shear strain rate are difficult to assess because the strain rates themselves are so small. However, there are a handful of noteworthy changes. First of all, the strain rates at G1a and G2a have decreased at both margins and migrated outward at the northern margin. This pattern is what was expected based on the changes observed in the velocity profiles. WIS1 shows minimal changes, with a slight increase in strain rate at G1b. Finally, the deceleration and narrowing of G4 is shown as a decrease and narrowing of the strain rate.

### 4.4 Shear Stress Variations

The shear stress variations basically mimic the strain rate changes. Shear stress,  $\sigma_{ij}$ , is related to the shear strain rate,  $\dot{\epsilon}_{ij}$ , using Glen's flow law. This is the conventional non-linear flow law used for glacier ice. A fundamental aspect of Glen's flow law is that any specific strain rate is not only a function of the stress in that specific direction, but also of all the other stresses acting on the medium. It is important to point out, therefore, that the effective strain rate and shear stress were originally used in this equation. However, since the contribution of the other strain rates is negligible, equation (3) can be used:

$$\dot{\epsilon}_{ij} = \left( \frac{\sigma_{ij}}{B} \right)^n \quad (3)$$

Where B is a viscosity parameter that increases with depth, and n is a constant equal to 3. Shear stress variations are shown in Figure 13.

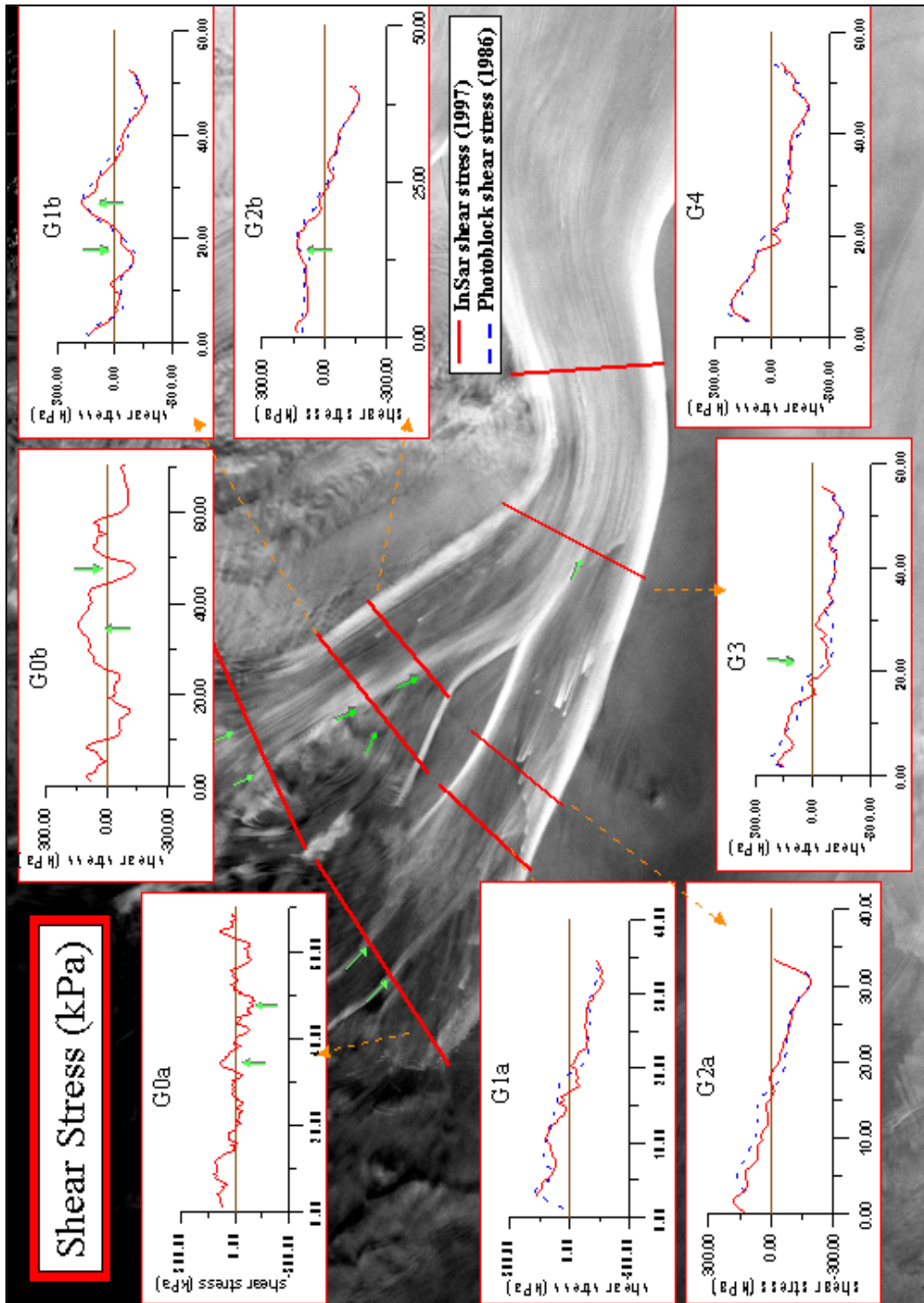


Figure 13: Shear stress variations across Whillans Ice Stream. Solid (red) lines are from InSAR results; dashed (blue) lines are from Photoblock results.

#### *4.4.1 Spatial Variations in Shear Stress*

The shear stress shows a similar pattern that the strain rates show, but they are amplified because they are multiplied by the rate factor. At the catchments, the signals made by the linear flow stripes are more noticeable, as shown by the green arrows. The complex pattern of shear stress at the catchments is indicative of the complex flow structure in this area. Further downflow where the ice stream is well developed, the shear stress portrays a characteristic signal: positive at one shear margin, zero at the centerline, negative at the opposing shear margin. This pattern is displayed at the WIS2 transects. Deviations from this pattern are noticeable in WIS1, due to the merging tributary from the south. At G3, a noticeable anomaly is that the shear stress reaches zero off-center. The shift from positive to negative shear stress occurs closer to the north margin than the south margin. This shift is pointed out by the green arrow, which shows the transition from WIS2 to WIS1 ice.

#### *4.4.2 Temporal Variations in Shear Stress*

Temporal variations along WIS2 show the expected decrease related to velocity and widening of the northern margin. A noticeable aspect of these profiles is that the southern half of the ice stream changes very little. The decrease in shear stress is only significant slightly before the centerline.

#### 4.5 Implications/Explanations of Spatial and Temporal Changes

The general trend of Whillans Ice Stream is that it is decelerating over time. This trend is most noticeable along the northern portion of the ice stream. As it is decelerating, strain rates and shear stresses at the margins are decreasing. This is especially true at the southern margins. Conversely, there is little change along the northern tributary, both in terms of velocity and margin change.

Over the past ten years, the Whillans Ice Stream has become more symmetric after WIS1 and WIS2 merge. The deceleration of WIS2 has led to a smoother convergence of the two tributaries. As the entire ice stream decelerates, not enough strain is available at the margins and narrowing occurs near gate G4. The DISP imagery suggests that 34 years ago, WIS2 was even more robust. It has clearly slowed down and gotten a lot narrower over time. Further investigations into the mass balance and force budget of Whillans Ice Stream will provide more insight into the possible causes of these observed changes.

## CHAPTER 5

### MASS BALANCE AND FORCE BUDGET

#### 5.0 Goals

Mass balance and force budget calculations are often used to determine the health of a glacier. The results described in Chapter 4 can be used to complete these calculations for Whillans Ice Stream. By combining mass balance and force budget investigations, a complete picture of the flow dynamics can be made.

#### 5.1 Mass Balance

Mass balance studies investigate spatial and temporal changes of glacier's mass, determined by comparing mass input with mass output. Such studies are often used to make a fundamental link between a glacier's behavior and changes in climate. This process has been conducted at various scales from local, such as the Byrd Station Strain Network (Whillans, 1977) to very large scales, such as for all of Antarctica (Bull, 1971). In this study the mass balance of a single drainage basin, Whillans Ice Stream, is investigated, assuming mass conservation. The input is from snow accumulation and ice flow above a gate, and the output is calculated from flow out of the gate and basal melting. The location of flux gates along the ice stream was shown in Figure 9.

The lateral boundaries of these ice streams are defined by shear margins where applicable, and along flowlines where shear margins are not present (such as for gates G00a and G00b). Ice does not flow transverse to flowlines and there is minimal flow across shear margins, so defining these features as lateral boundaries is appropriate.

Previous studies find a negative mass balance when investigating this ice stream (Joughin and Tulaczyk, 2002; Shabtaie and Bentley, 1988a; Whillans and Bindschadler, 1988). The mass balance results from these studies were altered to account for only the main section of Whillans Ice Stream (G0-G4) that was considered in this study.

Information pertaining to the mass balance of the catchment and areas downstream from transect G4 were not included. Using scarce Transit velocity measurements, Shabtaie and Bentley (1988a) obtained a dramatic thinning rate of  $60 \pm 10$  cm/yr. Whillans and Bindschadler (1988) used a combination of Transit velocities to calculate the input flux and photogrammetry to calculate the output flux. Their results suggests a thinning rate of  $6.0 \pm 4$  cm/yr. Joughin and Tulaczyk (2002) found minimal change in mass balance over Whillans Ice Stream using InSar velocities. A table of the parameters used in each of these studies is shown in Section 5.1.3.

### ***5.1.1 Equations***

The basic equation for mass balance was used (equation 4) and adapted for streaming flow (equation 5). Assuming a constant mean density of  $917 \text{ kg/m}^3$ , the conservation of mass can be determined in terms of volume fluxes (Shabtaie and Bentley, 1988a). Figure 14 illustrates the role of each flux.

The fluxes coming in from the sides ( $F_r$  and  $F_l$ ) are negligible in this study because lateral boundaries of shear margins and flowlines were chosen. Figure 15 is a diagram of the terms used in equation (5). Only the shaded arrows represent values used in calculating the total flux.

$$F_{net} = F_{in} - F_{out} \quad (4)$$

$$F_{net} = F_{in} + F_r + F_l + F_s - F_b - F_{out} \quad (5)$$

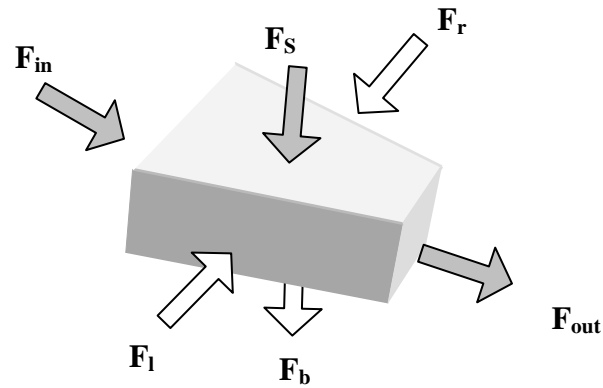


Figure 14: Illustration of terms used in equation (5)

Since basal melt rate,  $F_b$ , cannot be measured directly, it must be calculated using equation (6). This equation assumes that basal temperatures are at the pressure melting point, which is concordant with studies by Engelhardt and Kamb (1993). They found basal temperatures at UpB camp (on tributary WIS2) to be  $-0.82^\circ\text{C}$ , while the calculated pressure melting point for ice 1052 m thick is  $-0.70^\circ\text{C}$ . Surface temperatures do not vary significantly over ice streams and interstream ridges, but the relationship between basal temperatures and the pressure melting points do. Under ridges, the basal temperature is below the pressure melting point by  $0.6 - 2.7^\circ\text{C}$ , depending on the study site (Kamb et al., 2000). Figure 15 is a schematic of this process.

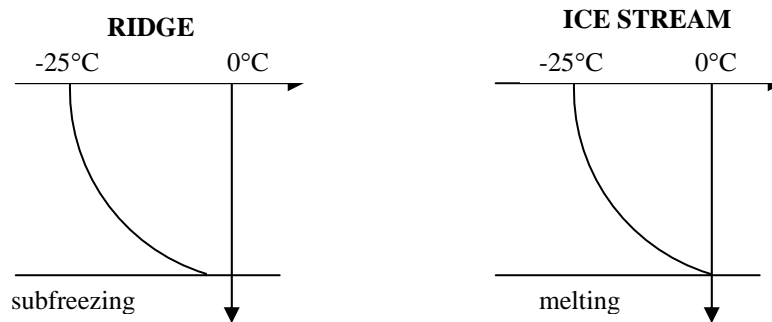


Figure 15. Vertical temperature profiles relative to the basal melting point, for a ridge and an ice stream (adapted from Jacobson and Raymond, 1998).

The basal melting rate, the left side of equation (6), is dependent on a number of variables (in order of their appearance in the equation): latent heat of fusion, conduction, strain heating, the geothermal heat flux, and potential heating. The terms used in the equation are described in Table 2.

$$\frac{\Delta H}{\Delta t} = \frac{1}{\rho\lambda} \left( K \frac{\partial T}{\partial z} - \int \dot{\epsilon}_{xz} \tau_{xz} dz - G - \tau_{bx} u \right) \quad (6)$$

	<b>Definition</b>	<b>Value</b>	<b>Reference</b>
$\rho$	Density of ice	917 kg/m <sup>3</sup>	
$\lambda$	Latent heat capacity of ice	3.20x 10 <sup>5</sup> J/kg	
$K$	Thermal conductivity of ice	2.1 W/mK	
$\partial T/\partial z$	Heat conducted up from base	0.04 K/m	Engelhardt (1990)
$\epsilon_{xz}$	Vertical strain rate	~ 0.00	
$\tau_{xz}$	Vertical shear stress	2.0 kPa	
$G$	Geothermal heat flux	0.060 W/m <sup>2</sup>	Whillans (1988)
$\tau_{bx}^*$	Basal shear stress	6.5, 46.1, 2.9, 7.4, 2.2 kPa	Section 5.2.4
$u^*$	Average Velocity	200, 200, 400, 400, 800 m/yr	Section 3.1

\* Values refer to the area between transects G0a-G1a, G0b-G1b, G1a-G3a, G1b-G3b, G3-G4, respectively.

Table 2. Definition of terms in equation (3)

The strain heating term is minimal because it is integrated over the entire ice column. The geothermal gradient,  $G$ , is dependent on the bedrock underlying the ice stream. Old ocean floor has a typical heat flux of 0.060 W m<sup>-2</sup>, whereas continental crust is usually 0.057 W m<sup>-2</sup>. Marie Byrd Land, which underlies Whillans Ice Stream, is a

combination of old ocean floor and continents, so a round number of  $0.060 \text{ W m}^{-2}$  was used. This value is used in similar studies by Whillans and Bindschadler (1988) and Lingle and Brown (1987). Frictional heating is described by the last term. This term will vary depending on the basal drag and velocity in each area of the ice stream. The calculation for basal drag is described in detail in Section 5.2.4.

Basal melting ( $F_b$ ) was calculated for different areas of Whillans Ice Stream, with values ranging from 2-30 mm/yr. These values are significantly less than the errors associated with each flux and are therefore ignored. Basal melting was calculated for each area of the ice stream, as described in Table 3.

Transect	Velocity (m/yr) '86/'97	basal drag 1986 (kPa)	basal drag 1997 (kPa)	melt rate '86 (mm/yr)	melt rate '97 (mm/yr)
G0a-G1a	200		6.5 (1.0)		2.2 (0.2)
G0b-G1b	200		46.1 (1.2)		29.0 (0.1)
G1a-G3a	460 / 410	1.1 (1.6)	2.9 (1.7)	0.4 (1.4)	1.9 (0.6)
G1b-G3b	350 / 350	7.5 (1.2)	7.4 (1.6)	6.7 (0.2)	6.6 (0.2)
G3-G4	850 / 760	1.4 (1.0)	2.2 (1.0)	2.0 (0.7)	3.5 (0.5)

Table 3. Melt rate calculated for sections of WIS.

Even at its maximum (29 mm/yr at the catchment of WIS1), the basal melt rate is small enough to ignore in flux calculations. The melt rate is much smaller than the error limits assigned to each mass balance flux value.

The change in melt production over the eleven years of this study is not statistically different. While the magnitude of the melt rate does appear to increase over time, the results are small compared with the uncertainties. The parameters used to calculate basal drag are shown in Section 5.2, Table 5.

### ***5.1.2 Error Estimates***

The origin of individual error estimates for InSAR and Photoblock velocities and ice thickness are described in more detail in Chapter 3. Other errors that must be taken into account when calculating the mass balance are the accumulation rate and the area between each input/output gate. The error associated with accumulation is 15% (Venteris and Whillans, 1998) and does not vary much over Whillans Ice Stream. Determining the area between each flux gate is done using computer software. Repeat trials of this task indicate that the uncertainty is due to the subjective assessment of the margin location. Specifically, we chose the shear margins to be equivalent to flowlines, but this may not be the case. If there is advection of additional material across the shear margin then there could be additional (and unaccounted for) mass flux in the results. Velocity and ice thickness errors are responsible for the majority of the uncertainties in the mass balance results.

### ***5.1.3 Mass Balance Results***

The fluxes calculated using equation (4) for each gate are shown in Appendix B. To minimize the uncertainties, combinations of gates were used for analysis. Comparisons between the two data sets are limited by the location of the Photoblock data. For the Photoblock data set, the flux differences between gates G1a-G4a and G1b-G4b were used. The '20-block', which is located over gate G3, does not extend across the entire ice stream. As a result, the WIS1 half of the velocity profile was constructed entirely from interpolation. The results are included in the final diagrams of mass balance change, but should be viewed with caution.

The InSar data set is spatially extensive compared to the photoblocks. While it was of paramount interest to have identical gates over both data sets, additional ones were drawn as well. Gates G0a-G1a, G0b-G1b, G1a-G3a, G1b-G3b, G1a-G4a, G1b-G4b and G3-G4 were all investigated. In both data sets, the statistical differences between G1 and G2 were minimal, so these results are not included.

Figures 16 and 17 illustrate the changes in flux rate over time. The results are described for the individual tributaries and then for the entire ice stream. The errors associated with the mass balance results are propagated from velocity, ice thickness, accumulation rate and surface area uncertainties.

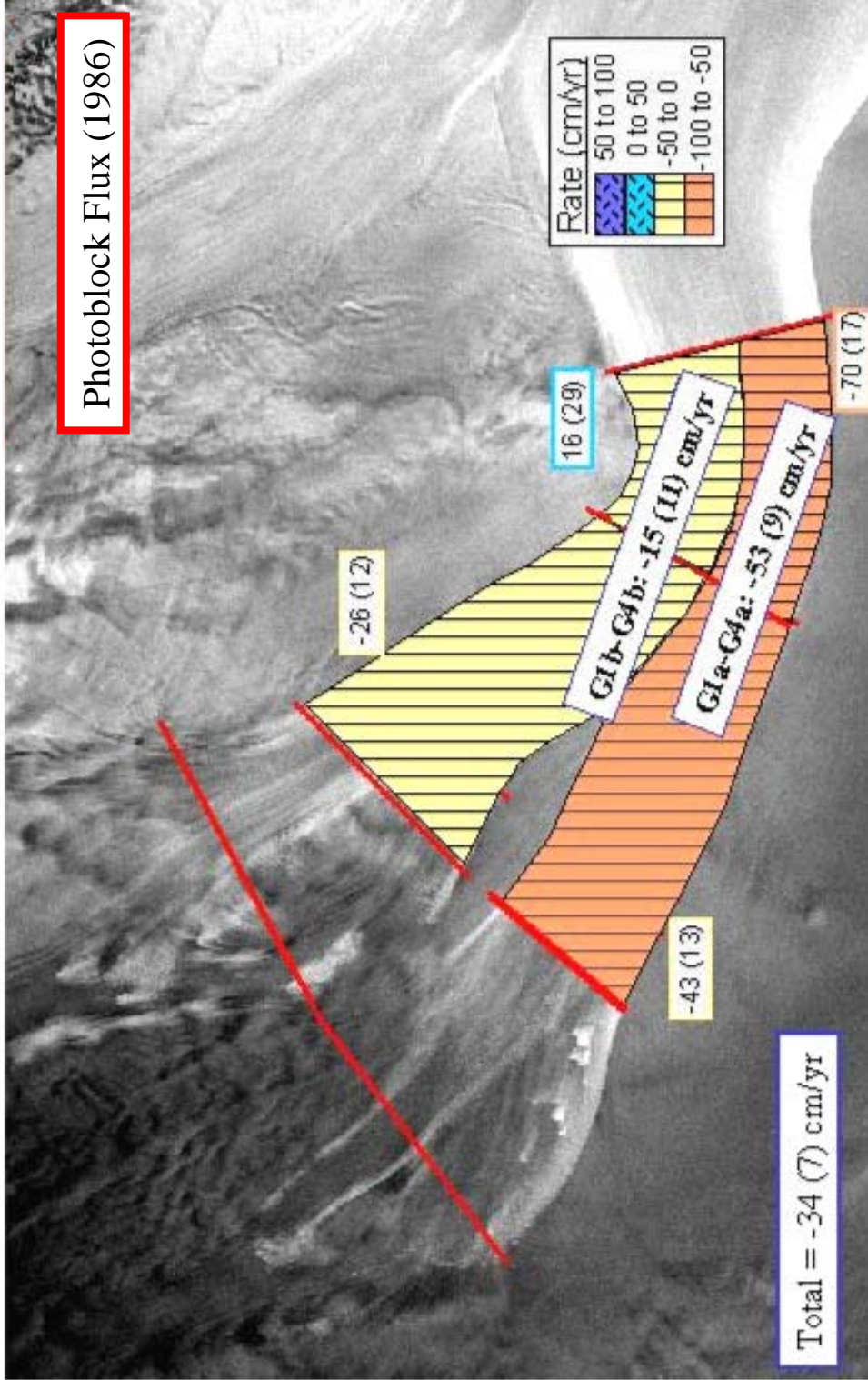


Figure 16: Flux rates (cm/yr) calculated using Photoblock velocities.

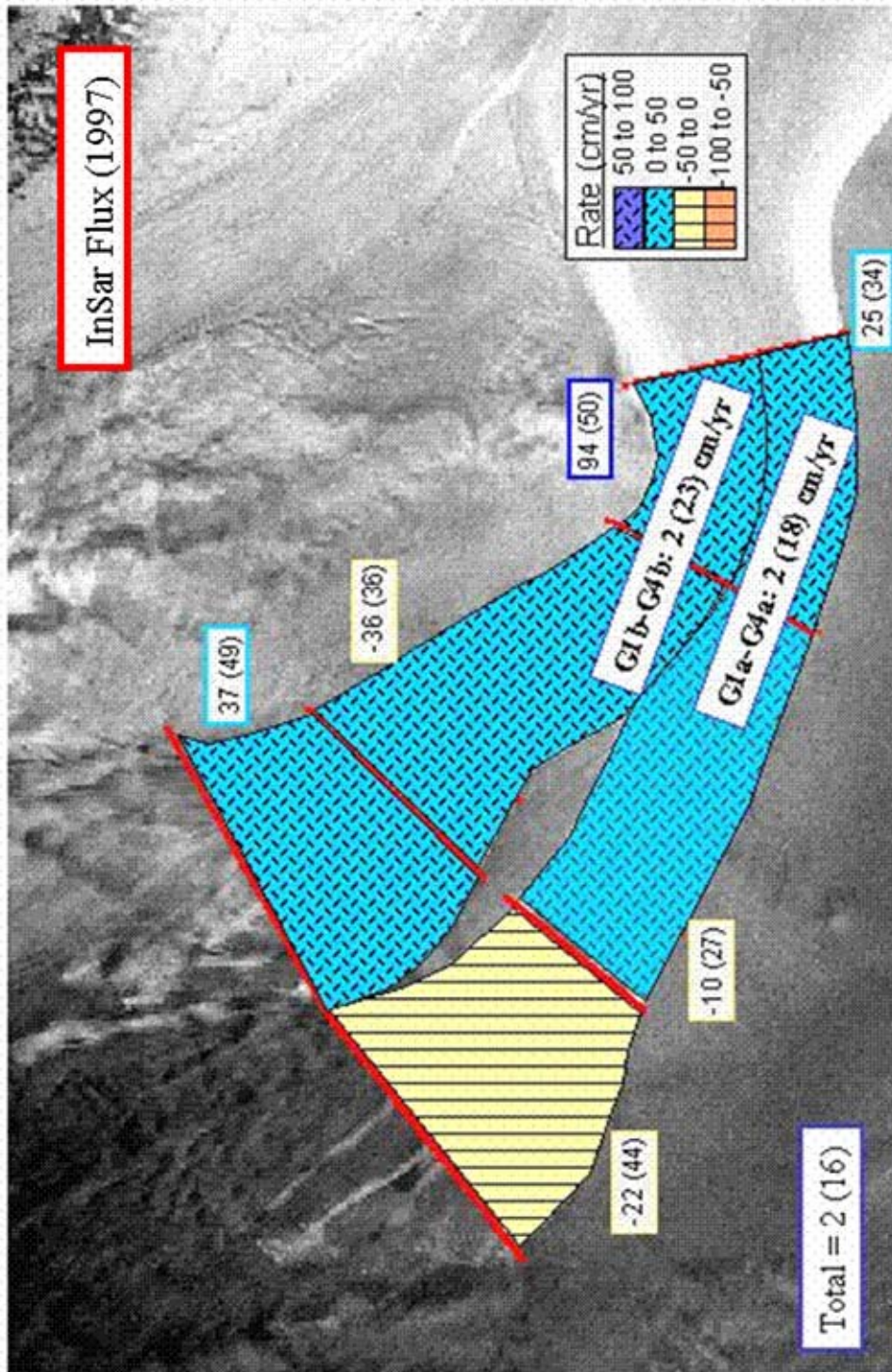


Figure 17: : Flux rates (cm/yr) calculated using InSar velocities.

### *5.1.3.1 Tributary B2*

During the late 1980s, Tributary B2 (herein referred to as WIS2) was thinning. While the entire tributary was thinning during this time, the area closest to the grounding line (gate G4) shows the most pronounced thinning at  $-70 (\pm 17)$  cm/yr (Figure 16). In contrast, the 1997 results show that this area is not significantly changing. The associated velocity profiles were shown in Figure 9. Near gate G4 there is a velocity decrease of approximately 100 m/yr coinciding with a narrowing of the northern margin by  $\sim 2.0$  km from 1986 to 1997. Gate G3 shows a similar pattern of change.

The WIS2 tributary appears to be closely linked to the behavior of the distal end of the ice stream (Figure 18). There is a general thinning trend in both 1986 and 1997, but the character of G4 affects the pattern of negative mass balance. In 1986, when the downstream area is thinning dramatically WIS2 is also thinning, although at a slower rate upstream. In 1997, when the far end of the ice stream trend is toward thickening, there is a propagation of this pattern upstream. Sequentially less thickening occurs upstream, with thinning still occurring at the catchment. Figure 18 shows the temporal changes of WIS2 at each gate. While the individual errors are large, there is a significant trend of the 1997 InSAR data of thickening at the margins.

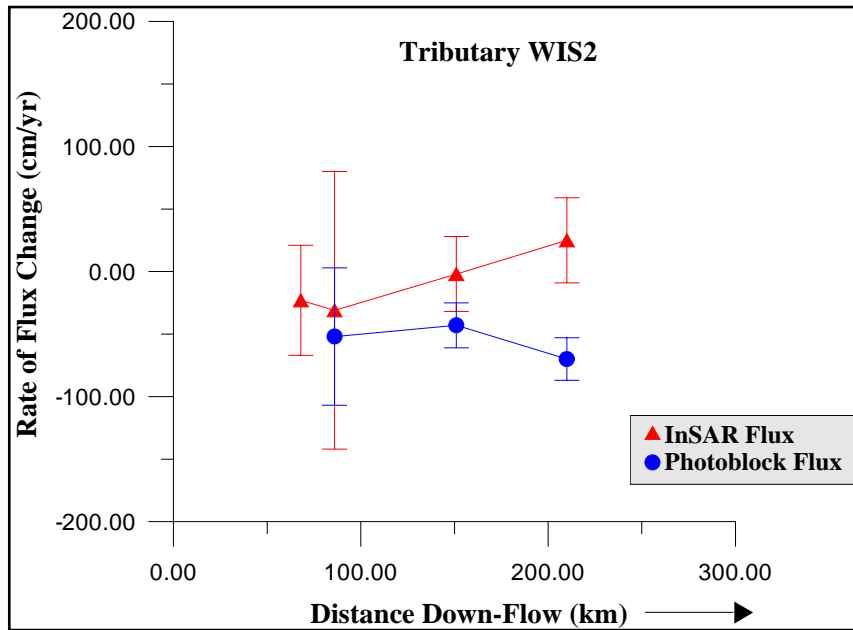


Figure 18: Temporal changes in mass balance along WIS2.

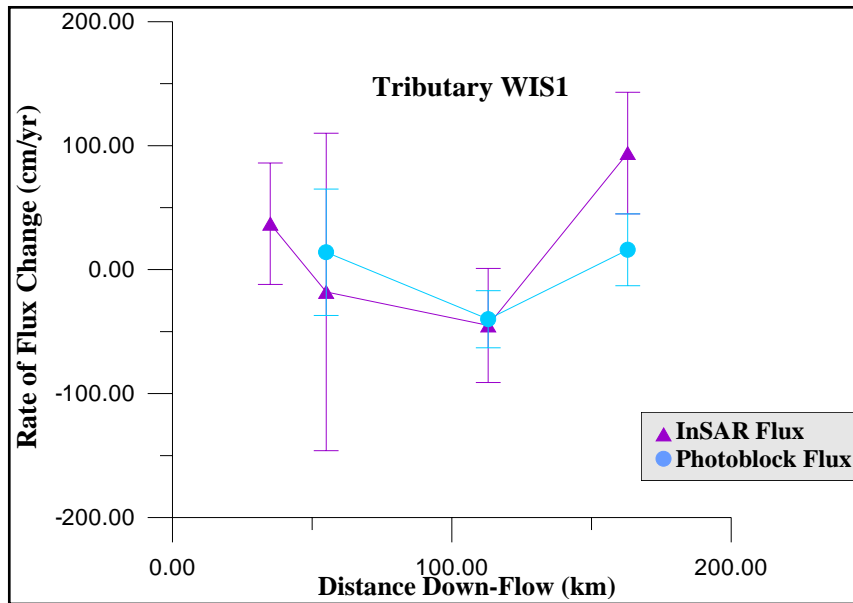


Figure 19: Temporal changes in mass balance along WIS1.

### *5.1.3.2 Tributary B1*

Tributary B1 (WIS1), the southern tributary, responds differently to changes down-glacier than its northern counterpart. The velocity profiles on WIS1 are not statistically different from 1986 to 1997. There is a slight decrease in velocity that is most noticeable at the centerline, with no significant change in the margin location. The location of the 10-block on WIS1 is complicated by the influx of a small tributary, which clouds the location of the margin. However, it is fairly evident that the margins of WIS1 are relatively fixed, especially in comparison to WIS2. The changes that occur from 1986 to 1997 are mostly due to changes that occur after the tributaries merge. Figure 19 illustrates the changes that have occurred along this tributary.

In 1986, the entire tributary from G1 to G4 is thinning. If G3 is considered, the tributary can be analyzed longitudinally. Similar to WIS2, WIS1 thins less upstream.

In 1997, the changes in WIS1 are more complicated. In addition, the large errors, unfortunately cloud the results. The catchment area and the middle portion of the ice stream are not statistically different and appear to be thinning, while the far end is thickening dramatically by  $94 (\pm 50)$  cm/yr. This gives the impression that ice is piling up at the distal end of the ice stream but still draining quickly out of the tributary. It is possible that WIS1 is more sensitive to changes at the grounding line, since it is topographically controlled and does not adjust for changes in velocity by margin migration.

### 5.1.3.3 Whillans Ice Stream

The thinning rate for the entire ice stream, determined by comparing the most upstream gate with the most down-stream gate, is  $-34 \pm 7$  cm/yr for 1986 and  $2 \pm 16$  cm/yr for 1997. Most of the changes are in the downstream region, by gate 4. Upstream of this area, thinning is apparent in WIS2 especially.

Author	Area (1000 km <sup>2</sup> )	Accumulation (cm/yr)	Input Flux (km <sup>3</sup> /yr)	Discharge (km <sup>3</sup> /yr)	Output longitude	Rate (cm/yr)
Shabtaie and Bentley (1988a) <sup>1</sup>	$20 \pm 2^*$	$10.9 \pm 3.8^*$	$15.8 \pm 5.8^*$	$26.22 \pm 1.3^*$	147 ° W	$-60 \pm 10^*$
Whillans and Bindschadler (1988)	$147 \pm 17$	14.3	$21.4 \pm 5.2$	$30.0 \pm 1.0$	147 ° W	$-6 \pm 4$
Joughin and Tulaczyk (2002) <sup>2</sup>	163	16.3	19.1	20.4	140 ° W	-0.9
Photoblocks <sup>3</sup>	7.6	$12 \pm .01$	$24.55 \pm 0.3$	$26.79 \pm 0.5$	147 ° W	$-34 \pm 7$
Insar <sup>4</sup>	12.3	$12 \pm .01$	$24.91 \pm 1.7$	$24.60 \pm 0.7$	147 ° W	$2 \pm 16$

\* using  $\pm$  limits as twice the standard error

<sup>1</sup> flux between their gates G0-G4

<sup>2</sup> flux estimate of WIS was isolated by subtracting ISA from the estimate of 'Ice Stream A and Whillans Ice Stream'. This result is for the area between Whillans B1 and B2 and where WIS and ISA merge (essentially G2 to the end of WIS1).

<sup>3</sup> flux between gates G1-G4

<sup>4</sup> flux between gates G0-G4

Table 4. Estimates of flux of Whillans Ice Stream

The variable results in Table 4 can be explained by taking a detailed look at each group's data set and method of analysis. For example, the study by Shabtaie and Bentley (1988a) should produce similar results to the photoblocks, since both studies analyzed flow across identical flux gates in the late 1980s. However, Shabtaie and Bentley

concluded that Whillans Ice Stream was thinning much more dramatically than the results from this study. The main difference between the two investigations can be attributed to the different velocity data sets. Shabtaie and Bentley used repeat ground-based Transit measurements collected by Whillans et al (1987). As a result, their velocity profiles across each gate rely on only three data points. The difference between their interpolated velocity profile for gate G4, and the velocity profile derived from photoblock velocities is shown in Figure 20. They are quite variable. This explains why Shabtaie and Bentley's mass balance results for Whillans Ice Stream in 1986 are different from those determined from the photoblocks (also 1986) in this study.

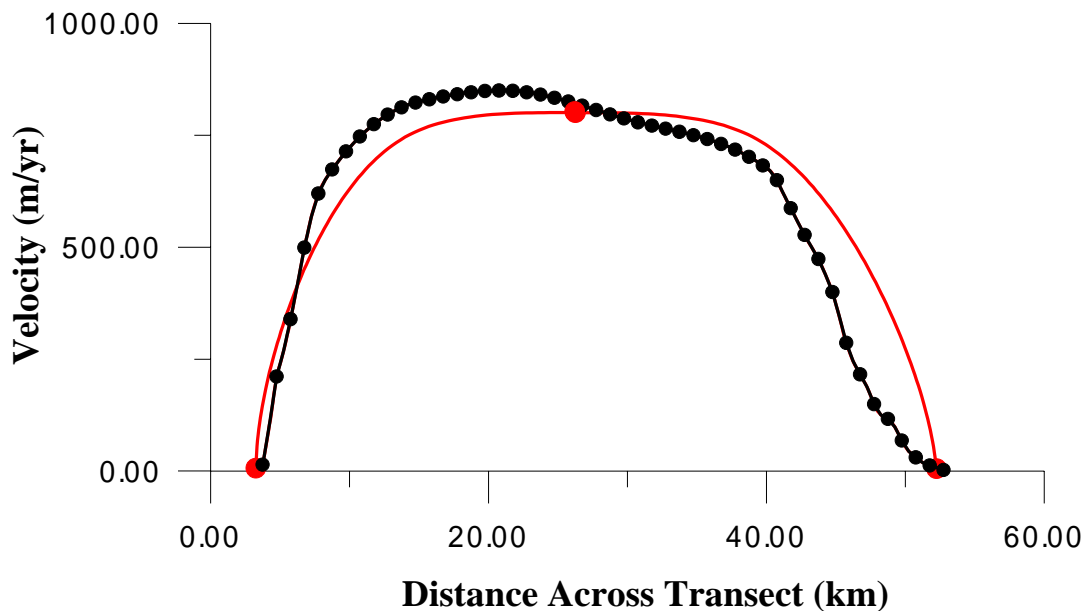


Figure 20: The velocity profile (smooth black line) used in this study, derived from photogrammetry compared to the velocity profile used in Shabtaie and Bentley's (1988a) mass balance investigation (red line). The bullets indicate the actual data points used in each study.

Whillans and Bindschadler (1988) used the '40-block' (also used in this study) to derive velocities for their output flux gate. The difference between their final result and the one suggested in this paper is due mainly to area. They assessed the flux for the entire catchment area of Whillans Ice Stream, while this study examines a much smaller area (from G1-G4). Uncertainties in estimating the location of the catchment and in determining precise accumulation rates are more significant in their study.

The difference of area is also responsible for the difference between the InSAR results from this study and Joughin and Tulaczyk's (2002) results, which used the same data set. Joughin's results were manipulated to isolate the area between gates B2 and B1 (which match the G2 gates used in this and Shabtaie and Bentley's study). The different location of both input and output gates, explains the slight difference between the two results.

## 5.2 Force Budget Technique

The large scale mechanics controlling glacier flow can be assessed by calculating the action effect of gravity, the driving stress, and the subsequent resistance to it. Resistance can come from the bed, from the sides, or from along-flow obstacles. Every component of the force budget can be calculated from velocity measurements, except for basal resistance. The driving stress is calculated from the geometry of the glacier; lateral and along-flow resistance can be derived from strain rates. Basal resistance is assumed to be the remaining imbalance in equation (7).

$$\tau_{dx} = \tau_{bx} - \frac{\partial}{\partial x} HR_{xx} - \frac{\partial}{\partial y} HR_{xy} \quad (7)$$

The forces in the down-glacier x-direction are considered in equation (7). The driving stress,  $\tau_{dx}$ , is balanced by resistive stresses basal drag, differential longitudinal tension and differential lateral drag, respectively (Whillans et al., 2000). The force budget technique uses a simple block-flow model, therefore assuming that stresses and strain rates are constant throughout the ice thickness (Van der Veen, 1999). As a result, velocity measurements taken at the surface can be applied for the whole ice column.

Figure 21 is a schematic of each of these forces.

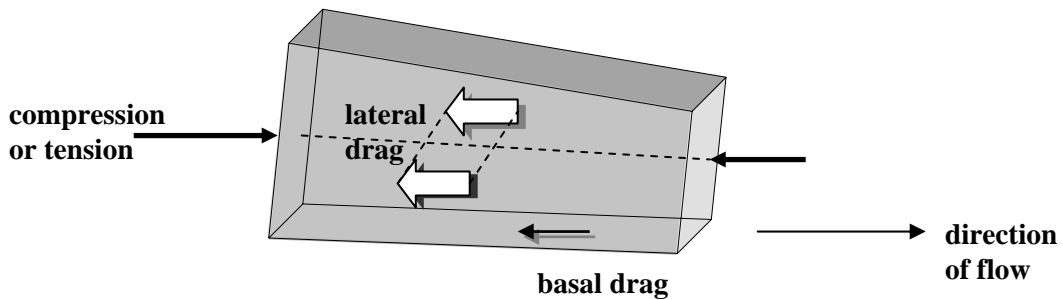


Figure 21. The location of resistive forces opposing glacier flow.

Resistive stresses described in Figure 21, are linked to deviatoric stresses,  $\sigma'_{ij}$ , as described by Whillans and Van der Veen (1989a).

$$\begin{aligned} R_{xx} &= 2\sigma'_{xx} + \sigma'_{yy} + R_{zz} \\ R_{xy} &= \sigma'_{xy} \end{aligned} \quad (8)$$

Deviatoric stresses are related to strain rates ( $\dot{\mathcal{E}}_{ij}$ ) through the conventional constitutive relation (Hooke, 1981).

$$\begin{aligned} \sigma'_{ij} &= B\dot{\mathcal{E}}_e^{(\frac{1}{n}-1)}\dot{\mathcal{E}}_{ij} \\ \dot{\mathcal{E}}_e^2 &= \frac{1}{2}\dot{\mathcal{E}}_{ij}\dot{\mathcal{E}}_{ij} \end{aligned} \quad (9)$$

The derivation of each component of resistive stress will be described separately.

### **5.2.1 Driving Stress**

Glacier motion is driven by the driving stress,  $\tau_{dx}$ , which describes how gravity interacts with the geometry of the glacier to cause acceleration. It is calculated from the product of surface slope ( $\partial h/\partial x$ ), ice thickness ( $H$ ), ice density ( $\rho$ ) and acceleration due to gravity, ( $g$ ).

$$\tau_{dx} = -\rho g H \frac{\partial h}{\partial x} \quad (10)$$

The driving stress along Whillans Ice Stream is shown in Figure 22. These calculations rely on the OSUDEM for the surface slope and BEDMAP for the ice thickness (Figure 22). Most previous studies have considered flowlines along WIS2, where the UpB camp is located. Along this tributary, the driving stress is approximately 14 kPa. However, WIS1, has more of a surface slope and maintains a driving stress that is slightly larger than WIS2. The average of each respective driving stress (from Gate 0 to Gate 4) is 13 kPa for WIS2 and 17 kPa for WIS1. The catchment of WIS1 has a significantly steeper surface slope, explaining its high driving stress.

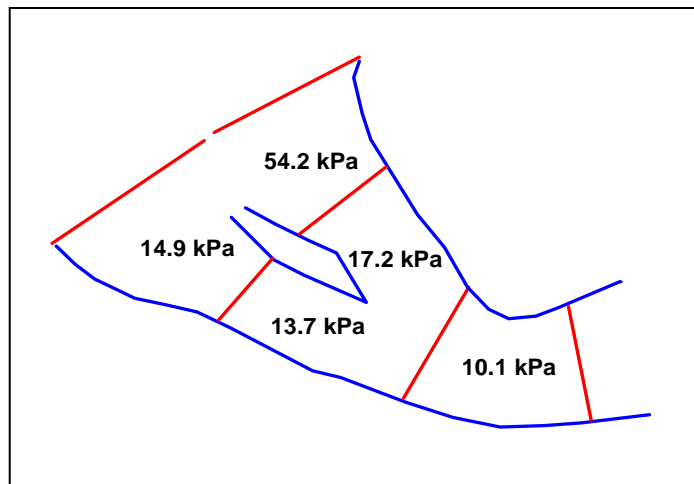


Figure 22. Distribution of the driving stress along Whillans Ice Stream. The driving stress was calculated for each area of the ice stream, as delineated by the transverse lines.

### 5.2.2 Longitudinal Tension / Compression

The longitudinal component of equation (7) describes the differential longitudinal tension along the ice stream. It is evaluated using a combination of longitudinal and transverse stretching rates and the constitutive relation for ice. Longitudinal stretching is derived from velocity measurements along the ice stream centerline (Whillans et al., 2000).

$$\dot{\epsilon}_{xx} = \frac{\partial U_{\max}}{\partial x} \quad (11)$$

The transverse strain rate is determined by computing longitudinal variations in ice stream width, W.

$$\dot{\epsilon}_{yy} = \frac{\partial W}{\partial y} \quad (12)$$

Using the constitutive relation, the longitudinal tension can be calculated from equation (13).

$$R_{xx} = B \epsilon_e^{-\frac{2}{3}} \left[ 2\dot{\epsilon}_{xx} + \dot{\epsilon}_{yy} \right] \quad (13)$$

A depth-averaged rate factor,  $B$ , of  $540 \text{ kPa/yr}^{1/3}$  is used, based on borehole temperature measurements near UpB camp (Engelhardt et al., 1990). This value corresponds to a depth-averaged temperature of  $-18^\circ\text{C}$ . The exponent  $n$  used in the flow law is 3. This equation assumes that velocities do not change much with depth (Whillans and Van der Veen, 1993).

Whillans and Van der Veen (1993b) conducted a thorough analysis of variations in longitudinal stresses along Whillans Ice Stream. They found a negligible gradient in longitudinal stresses along the ice stream. As a result, this study considers longitudinal components to be negligible in force balance calculations.

### ***5.2.3 Lateral Drag***

Resistance to flow from lateral drag can be assessed by determining how the lateral shear stress,  $R_{xy}$ , varies across the ice stream. The shear stress is derived from the shear strain rate using the inverse formulation of Glen's flow law for glacier ice.

$$R_{xy} = B \left( \frac{1}{2} \frac{\partial U}{\partial y} \right)^{\frac{1}{3}} \quad (14)$$

This equation assumes that  $\dot{\epsilon}_{xy}$  is the dominant strain rate, so that the shearing rate can replace the effective strain rate. Whillans et al. (1993) proved that longitudinal tension and lateral compression are negligible, validating this assumption (especially near the UpB camp).

The lateral resistance on a section of the ice stream can be determined from equation (15). The lateral shear stress at the margin is  $\tau_s$  and the thickness at the margin is  $H_w$ .

$$F_s = \frac{H_w \tau_s}{W} \quad (15)$$

Variations in  $\tau_s$  both down-flow and for adjacent margins were described in Section 4.4 of this study. In both tributaries, the northern margin has a consistently higher shear stress than the southern one, with the exception of Gates 1 and 2.

#### **5.2.4 Basal Drag**

Since it is not possible to calculate basal drag directly, it can be determined as the residual of the right hand side of equation (7). Computed this way, basal drag is very small (Whillans et al., 1997). Along the ice stream, basal drag varies from large values at the onset (where longitudinal and lateral forces gradients are small) to insignificant values along the majority of the ice stream.

Calculating the width averaged force balance, equations (7) and (15) are combined to form equation (16). It is assumed that the lateral shear stress is constant with depth and that longitudinal stress gradients can be ignored. The overbar represents an averaged value (Van der Veen, 1999).

$$\bar{\tau}_{dx} = \bar{\tau}_{bx} + \frac{H_w \tau_s}{W} \quad (16)$$

Table 5 lists the values used and the resulting force budget components along Whillans Ice Stream in 1986 and 1997. Transects with the suffix ‘a’ refer to WIS2 transects; those that end in ‘b’ refer to transects along WIS1.

Transect	Length (km)	Width (2W)	Thickness (m)	Slope	$\tau_{dx}$ (kPa)	$F_s$ 1986	$F_s$ 1997	$\tau_{bx}$ 1986	$\tau_{bx}$ 1997
G0a-G1a	50	52 (4)	1131 (18)	0.00147	14.9 (0.2)		8.4 (1.1)		6.5 (1.1)
G0b-G1b	36.5	63 (5)	1502 (18)	0.00402	54.3 (0.7)		8.3 (1.0)		46.1 (1.2)
G1a-G3a	83.6	32 (2)	1038 (18)	0.00147	13.8 (0.2)	12.7 (1.6)	10.9 (1.7)	1.1 (1.6)	2.9 (1.7)
G1b-G3b	76	43 (3)	1252 (18)	0.00153	17.2 (0.2)	9.7 (1.2)	9.8 (1.6)	7.5 (1.2)	7.4 (1.6)
G3-G4	53	57 (4)	980 (18)	0.00115	10.1 (0.2)	8.7 (1.0)	7.9 (1.1)	1.4 (1.0)	2.2 (1.1)

Table 5. Force Budget along Whillans Ice Stream in 1986 and 1997. Associated errors are shown in parentheses.

These results suggest that previous conclusions about the importance of lateral drag in controlling Whillans Ice Stream could be accurate for WIS2 and the main trunk of the ice stream. However, WIS1, especially at the catchment, cannot be supported by lateral drag alone. Mechanisms at the bed, or longitudinal gradients must play a role.

### ***5.2.5 Spatial Changes in the Force Budget***

Values of calculated basal drag are not uniform throughout the ice stream. At the catchments, where surface relief is more prominent (especially along WIS1), the driving stress is higher while lateral drag does not increase. This results in high values for calculated basal drag, based on equation (17) (which assumes that longitudinal components of stress are negligible). Once the ice stream shear margins become well developed, the basal drag plays less of a role in resisting the driving stress. However, for WIS1, basal drag is still an important component, accounting for 44% of the driving stress.

Along WIS2 and the main part of the ice stream, basal drag is approximately 2 kPa, which agrees with estimates by Echelmeyer (1994), and Whillans and Van der Veen (1997). In these areas, basal drag opposes approximately 20% of the driving stress. The other 80% is provided by lateral drag. Along WIS1, however, lateral drag only opposed ~50% of the driving stress. The remainder of the resistances comes from some combination of basal drag and longitudinal compression. Interestingly, lateral drag is smaller after the two tributaries coalesce. If lateral drag was the dominant resistant force, the shear stress should double after WIS1 and WIS2 merge – or the velocity should increase. In this case, the absence of two shear margins, causes a near doubling of velocity. The total width of the ice stream decreases by 22 km after the two tributaries merge (from a total width of 78 km to 56 km). The decrease in lateral drag coincides with a narrowing of the ice stream and a substantial increase in velocity.

### ***5.2.6 Temporal Changes in the Force Budget***

The temporal changes in force budget portray the close relationship between changes at the terminus and WIS2. In both of these areas, the lateral shear stress has diminished since 1986. This change is due to the decrease in velocity, which has caused the slope of the velocity profile at the margins to level out. Based on equation (17), if the magnitude of lateral drag decreases, basal drag must increase (assuming the driving stress is constant). As a result, the calculated basal drag at the terminus and along WIS2 increases from 1986 to 1997. Whether or not this change in lateral drag translates to a realistic change in basal drag is hard to determine. However, the important aspect to note in these results is that there is a concomitant shift in WIS2 and the main portion of the ice stream. This observation is also noticed in the mass balance results. Thickening rates at the terminus appear to be related to changes along WIS2. WIS1 does not seem to be as sensitive to changes at the grounding line.

### **5.3 Conclusions**

The results from the mass balance and force budget calculations tell a consistent story about changes along Whillans Ice Stream. Mass balance assessments indicate substantial thickening in recent years, especially at the distal end of the ice stream. The thickening appears to be asymmetric, with more thickening occurring on the southern half (WIS1) of the ice stream. Evidence for this asymmetry is noticed from the surface topography and the mass balance results. The surface topography reveals a slight depression located near the northern portion of gate G4. This observation is consistent

with mass balance results that suggest that the southern portion of this area is thickening at a rate that is almost four times faster than the northern portion (94 cm/yr vs. 23 cm/yr).

Force budget results provide further insight into the complex behavior of Whillans Ice Stream. The calculated basal drag (see equation 17) from 1986 to 1997 implies that there is an increase in basal drag along WIS2 and at the distal end of the ice stream. If this result is real and not an artifact of the data, then the depletion of melt water at the base of the ice stream is most likely responsible for all of the changes observed. With a lack of basal meltwater along WIS2 and the terminus, basal drag will increase, deceleration will occur, the ice stream will thicken and margins will migrate.

## CHAPTER 6

### CONCLUSIONS

Over the past ten years, noticeable changes have occurred on Whillans Ice Stream. Investigations into the geometry, velocity, mass balance and force budget, all show the dynamic nature of the ice stream. The cause of these changes is not known conclusively, but can be hypothesized based on the described observations.

A close look at temporal velocity changes in Chapter 4 revealed a deceleration of ~ 50 m/yr along WIS2 and a deceleration of ~100 m/yr near gate G4. WIS2 is widening to the north at a rate of 200 m/yr and 50 m/yr to the south. This southward migration is consistent with other studies by Hamilton (1998) and Echelmeyer et al. (1998). In contrast, the main portion of the ice stream (gates G3 and G4) are slowing up to 100 m/yr and narrowing by 3-4 km in ten years. We speculate that the deceleration of these areas may be due to a loss of basal melt water, which would increase basal drag. An explanation for margin migrations occurring in opposite directions along the ice stream is still being investigated.

The mass balance of Whillans Ice Streams indicates that thickening is occurring at the terminus. These thickening rates are more pronounced on the southern side of the ice stream, after WIS1 and WIS2 merge. In addition, the northern side of WIS was thinning at 70 cm/yr in 1986. Consequently, the surface topography of the northern part of the ice

stream should be lower than the southern part. A close look at the surface DEM, reveals this expected result (Figure 23). There is a surficial trough that trends up WIS2, that may be due to the measured contrast in mass balance results across the ice stream.

The force budget technique showed a distinct spatial pattern along the ice stream. Previous studies have suggested that lateral drag is the main resistant force in Whillans Ice Stream. While this statement is probably accurate for WIS2, it does not apply to WIS1 where lateral drag only accounts for 50% of the driving stress. The rest of the resistance comes from some combination of longitudinal stress and basal drag. Longitudinal stress gradients along this tributary need to be determined before conclusions are drawn as to which stress is most critical here.

The observations suggest that either basal drag is increasing over time or the driving stress is decreasing. An increase in basal drag may be due to a decrease in the amount of melt water that is present at the base. The difference in calculated melt water production using the basal drag and surface velocity data for 1986 and 1997 is only 1.5 mm/yr (Table 3). This result suggests that observed changes on Whillans Ice Stream are due to a 'weakening' of the driving stress. Future work will be done to calculate the predicted change in driving stress based on the mass balance results (which would alter the down-glacier slope).

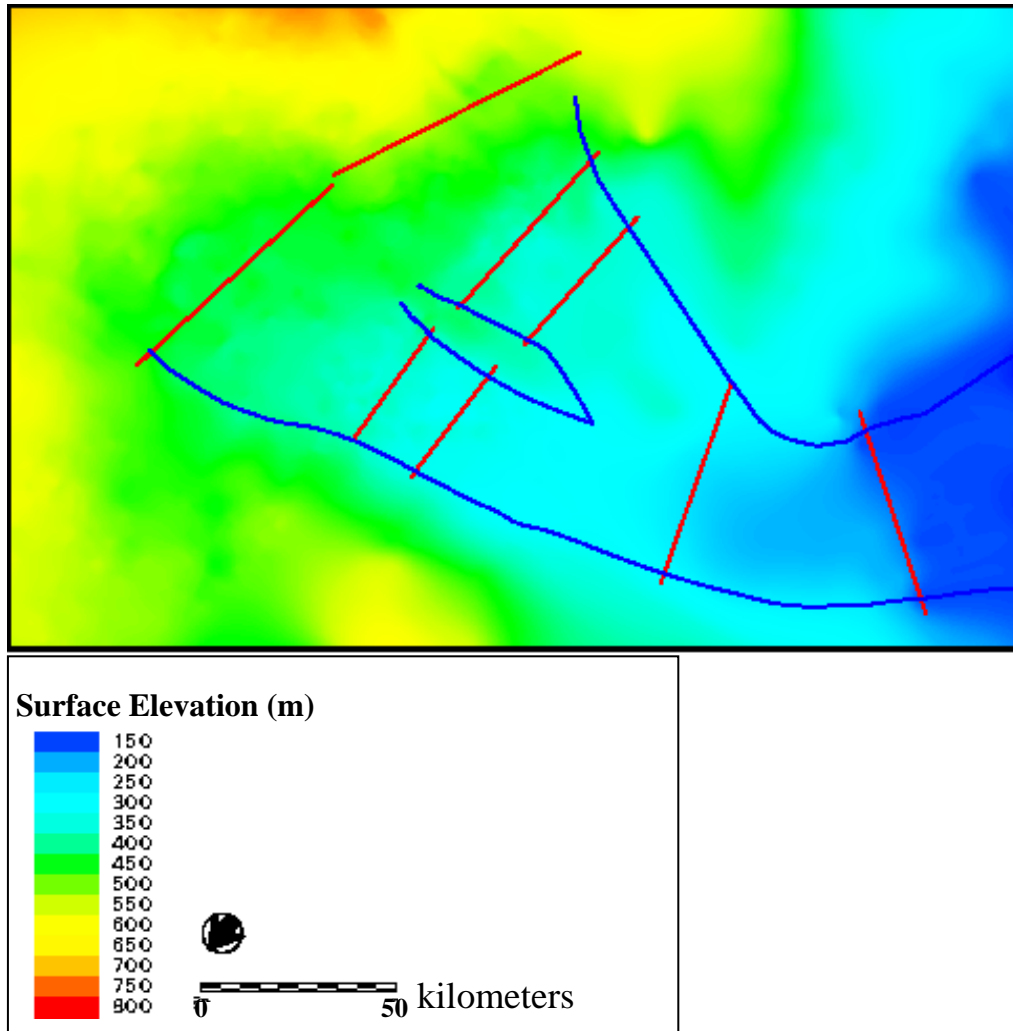


Figure 23: OSUDEM of Whillans Ice Stream, showing a substantial surface depression that trends up WIS2 from the down-stream end of the ice stream.

## REFERENCES

- Alley, R.B., D.D. Blankenship, C.R. Bentley, and S.T. Rooney. (1986). Deformation of till beneath Ice Stream B, West Antarctica, *Nature*, 322, 57-59.
- Alley, R.B. and I.M. Whillans. (1991). Changes in the West Antarctic Ice Sheet, *Science*, 254, 959-963.
- Bentley, C.R. (1987). Antarctic ice streams: A Review, *Journal of Geophysical Research*, 92(B9), 8843-8868.
- Bindschadler, R.A., S.N. Stephenson, D.R. MacAyeal, and S. Shabtaie. (1987). Ice dynamics at the mouth of Ice Stream B, Antarctica. *Journal of Geophysical Research*, 92, 8885-8894.
- Bindschadler, R. (1997). Actively surging West Antarctic ice streams and their response characteristics, *Annals of Glaciology*, 24, 409-414.
- Bindschadler, R. and P. Vornberger (1998). Changes in the West Antarctic ice sheet since 1963 from declassified satellite photography, *Science*, 279, 689-692.
- Bindschadler, R. and W. Seider. (1998). Declassified Intelligence Satellite Photography (DISP) Coverage of Antarctica, *NASA/TM – 1998-206879*, 37 pp.
- Blankenship, D.D. et al. 2000. Geologic controls on the initiation of rapid basal motion for West Antarctic ice streams: A geophysical perspective including new airborne radar sounding and laser altimetry results. *The West Antarctic Ice Sheet: Behavior and Environment, Antarctic Research Series*, 77, 105-121.
- Bull, C. (1971). Snow Accumulation in Antarctica. In Quam, L.O., ed. *Research in the Antarctic*. Washington, DC, American Association for the Advancement of Science, 367-421.
- Casassa, G., K.C. Jezek, J. Turner, and I.M. Whillans. (1991). Relict flow stripes on the Ross Ice Shelf, *Annals of Glaciology*, 15, 132-138.
- Echelmeyer, K.A. and W.D. Harrison. (1999). Ongoing margin migration of Ice Stream B, West Antarctica, *Journal of Glaciology*, 45, 361-369.

- Engelhardt, H., N. Humphrey, B. Kamb, and M. Fahnestock. (1990). Physical conditions at the base of a fast moving Antarctic ice stream, *Science*, 248, 57-59.
- Engelhardt, H.F. and B. Kamb. (1993). Vertical temperature profile of ice stream B, *Ant. Jnl. U.S.*, 28, 63-66.
- Engelhardt, H. and B. Kamb. 1998. Basal sliding of Ice Stream B, West Antarctica, *Jnl. Glaciology*, 44, 223-230.
- Forster, R.R., K.C. Jezek, H.G. Sohn, A.L. Gray and K.E. Matter. (1998). Analysis of Glacier Flow Dynamics from Preliminary RADARSAT InSAR Data of the Antarctic Mapping Mission. *IEEE*, 2225-2227.
- Greischar, L.L. and C.R. Bentley. 1980. Implications for the late Wisconsin/Holocene extent of the West Antarctic ice sheet from a regional isostatic gravity map of the Ross Embayment (Abstract). Sixth Biennial Meeting of AMQUA, Orono, Maine, August 18-20, 1980
- Hamilton, G.S., I.M. Whillans, and P.J. Morgan. (1998). First point measurements of ice-sheet thickness change in Antarctica, *Annals of Glaciology*, 27, 125-129.
- Hooke, R. LeB. (1981). Flow law for polycrystalline ice in glaciers: comparison of theoretical predictions, laboratory data, and field measurements, *Rev. Geophys. Space Phys.*, 19, 664-672.
- Hooke, R. LeB. (1998). *Principles of Glacier Mechanics*. Prentice Hall, New Jersey.
- Jackson, M. (1991). Repeat aerial photogrammetry of Ice Stream B, West Antarctica, Master's Thesis, The Ohio State University, 120 pp.
- Jacobson, H.P. and C.F. Raymond. 1998. Thermal effects on the location of ice stream margins. *Journal of Geophysical Research*, 103(B6), 12,111-12,122
- Jezek, K.C., J. Curlander, L. Norikane, F. Carsey, J.P. Crawford, C. Wales, J. Muller. (1996). RADARSAT: The Antarctic Mapping Project, *IEEE*, 1775-1776.
- Jezek, K.C., H.G. Sohn, and K.F. Noltimier. (1998a). The Radarsat Antarctic Mapping Project, *Proceeding of IGRSS*, Seattle.
- Jezek, K.C. et al. (1998b). Snapshots of Antarctica from RADARSAT -1, *IEEE*, 1428-1430.
- Jezek, K.C. (1999). Glaciological properties of the Antarctic ice sheet from RADARSAT-1 synthetic aperture radar imagery, *Annals of Glaciology*, 29, 286-290.

- Joughin, I. (1995). Estimation of Ice-Sheet Topography and Motion Using Interferometric Synthetic Aperture Radar, PhD. Thesis, University of Washington,
- Joughin, I. L. Gray, R. Bindshadler, S. Price, D. Morse, C. Hulbe, M. Karin, and C. Werner. (1999). Tributaries of West Antarctic ice streams by RADARSAT interferometry, *Science*, 286, 283-286.
- Joughin, I. and S. Tulaczyk. (2002). Positive Mass Balance of the Ross Ice Streams, West Antarctica. *Science*, 295, 476-480.
- Joughin, pers comm., 2002.
- Kamb, B. 2000. Basal zone of the West Antarctic Ice Streams and its role in lubrication of their rapid motion. *The West Antarctic Ice Sheet: Behavior and Environment, Antarctic Research Series*, 77, 157-199
- Kim, K. (1999). Application of time series satellite data to earth science problems, Master's Thesis, The Ohio State University, 69 pp.
- Lillesand, T.M. and R.W. Keifer. 2000. *Remote Sensing and Image Interpretation: Fourth Edition*. John Wiley and Sons, New York, 724 pp.
- Lingle, C.S. and T.J. Brown. (1987). S subglacial aquifer bed model and water pressure dependant basal sliding relationship for a West Antarctic ice stream. In: *Dynamic of the West Antarctic Ice Sheet*. C.J. van der Veen and J. Oerlemans (eds). Reidel, Dordrecht: 249-285.
- Liu, H. (1999). Development of an Antarctic Digital Elevation Model, *Byrd Polar Research Center*, Report No. 19, 157 pp.
- Liu, H., K.C. Jezek, L. Biyan. (1999b). Development of an Antarctic digital elevation model by integrating cartographic and remotely sensed data: A geographic information system based approach. *Journal of Geophysical Research*, 104:B10, 23,199-23,213.
- Lythe, M.B., Vaughan, D.G. and the BEDMAP Consortium. 2000. BEDMAP - bed topography of the Antarctic. 1:10,000,000 scale map. BAS (Misc) 9. Cambridge, British Antarctic Survey.
- McDonald, J. and I.M. Whillans. (1992). Search for temporal changes in the velocity of Ice Stream B, West Antarctica, *Journal of Glaciology*, 38:128, 157-161.
- McDonald, J. and I.M. Whillans. (1988). Comparison of results from Transit Satellite tracking, *Annals of Glaciology*, 11, 83-88.

- McDonald, R.A. (1995). CORONA – success for space reconnaissance, a look into the Cold War, and a revolution for intelligence: *Photogrammetric Engineering and Remote Sensing*, v. 61, no. 6, 689-720.
- Paterson, W.S.B. (1994). *The physics of glaciers*. Pergamon Press/Elsevier Ltd., Oxford, 3<sup>rd</sup> ed., 480 pp.
- Price, S. F., and I.M. Whillans. (1998). Delineation of a catchment boundary using velocity and elevation measurements, *Annals of Glaciology*, 27, 140-144.
- Price, S.F., R.A. Bindschadler, C.L. Hulbe and I.R. Joughin. (2001). Post-stagnation behavior in the upstream regions of Ice Stream C, West Antarctica, *Journal of Glaciology*, 47:157, 283-294.
- Raymond, C.F., K.A. Echelmeyer, I.M. Whillans and C.S.M. Doake. (2000). Ice Stream shear margins, *The West Antarctic Ice Sheet: Behavior and Environment, Antarctic Research Series*, 77, 137-155.
- Retzlaff, R. and C.R. Bentley. (1993). Timing of stagnation of ice stream C, West Antarctica, from short-pulse-radar studies of buried crevasses, *Journal of Glaciology*, 39, 553-561.
- Rose, K.E. (1979). Characteristics of ice flow in Marie Byrd Land, Antarctica, *Journal of Geophysical Research*, 24, 63-74.
- Scambos, T.A., K.A. Echelmeyer, M.A. Fahnestock, and R.A. Bindschadler. (1994). Development of enhanced ice flow at the southern margin of Ice Stream D, Antarctica. *Annals of Glaciology*, 20, 313-318.
- Shabtaie, S. and C.R. Bentley. (1987). West Antarctic ice streams draining into the Ross Ice Shelf: configuration and mass balance, *Journal of Geophysical Research*, 92, 1311-1336.
- Shabtaie, S., I.M. Whillans, and C.R. Bentley. (1987b). The morphology of ice streams A, B, and C, West Antarctica, and their environs, *Journal of Geophysical Research*, 92, 8865-8883.
- Shabtaie, S., C.R. Bentley, R.A. Bindschadler and D.R. MacAyeal. (1988). Mass-balance studies of ice streams A, B, and C, West Antarctica, and possible surging behavior of Ice Stream B. *Annals of Glaciology*, 11, 137-149.
- Shabtaie, S. and C.R. Bentley. (1988b). Ice-Thickness map of the West Antarctic ice streams by radar sounding, *Annals of Glaciology*, 11, 126-136.
- Thomas, R.H. and C.R. Bentley (1978). The Equilibrium State of the Eastern Half of the Ross Ice Shelf, *Journal of Glaciology*, 20:84, 509-518.

- Tulaczyk, S., W.B. Kamb, and H.F. Engelhardt. 2000a. Basal mechanics of Ice Stream B, West Antarctica. 1. Till mechanics. *Journal of Geophysical Research*, 105:B1, 463-481
- Tulaczyk, S., W.B. Kamb, and H.F. Engelhardt. 2000b. Basal mechanics of Ice Stream B, West Antarctica. 2. Undrained plastic bed model. *Journal of Geophysical Research*, 105:B1, 463-481
- Van der Veen, C.J. and I.M. Whillans. (1989b). Force Budget: II Application to two-dimensional flow along Byrd Station Strain Network, Antarctica. *Journal of Glaciology*, 35, 61-67.
- Van der Veen, C.J. (1999). *Fundamentals of Glacier Dynamics*. A.A.Balkema, Netherlands, 462 pp.
- Van der Veen, C.J. and I.M. Whillans. (1996). Model experiments on the evolution and stability of ice streams, *Annals of Glaciology*, 23, 129-137.
- Venteris, E.R. and I.M. Whillans (1998). Variability of accumulation rate in the catchments of ice streams B, C, D, and E, Antarctica, *Annals of Glaciology*, 27, 227-230.
- Whillans, I.M. (1975). Mass-balance and ice flow along the Byrd Station Strain Network, Antarctica, PhD Thesis, The Ohio State University, 141 pp.
- Whillans, I.M., J. Bolzan, and S. Shabtaie. (1987). Velocity of Ice Streams B and C, Antarctica. *Journal of Geophysical Research*, 92:B9, 8895-8902.
- Whillans, I.M. and R. Bindshadler. (1988). Mass balance of ice stream B, *Annals of Glaciology*, 11, 187-193.
- Whillans, I.M. and C.J. Van der Veen. (1993). Patterns of calculated basal drag on ice streams B and C, West Antarctica, *Journal of Glaciology*, 39, 437-446.
- Whillans, I.M. and C.J. Van der Veen. (1993b). New and improved determinations of velocity of ice streams B and C, West Antarctica, *Journal of Glaciology*, 39, 483-490..
- Whillans, I.M., M. Jackson, and Y-H. Tseng. (1993c). Velocity patterns in a transect across ice stream B, Antarctica. *Journal of Glaciology*, 39, 563-573.
- Whillans, I.M., C.R. Bentley, and C.J. Van der Veen. (2000). Ice Streams B and C. *The West Antarctic Ice Sheet: Behavior and Environment, Antarctic Research Series*, 77, 257-281.
- Zhao, Z. (2001). Surface velocities of the East Antarctic ice streams from Radarsat-1 interferometric synthetic aperture radar data. PhD. Thesis, The Ohio State University, 181 pp.

## APPENDIX A: PHOTOBLOCK ORIENTATION

Prior to my acquisition of the photoblocks, previous students of Dr. Whillans (Raid, Tseng, Jackson) had matched the time-sequential images, applied radiometric adjustments (equalization and noise reduction) and geometric corrections, and derived velocities from manual feature-tracking techniques.

However, the Photoblocks were each processed according to a unique local coordinate system and combining all the velocity information into a single polar stereographic grid proved to be an arduous task. Table A1 describes how each photoblock was rotated and incorporated into an X, Y stereographic system. As described in Section 3.2.3, a cross-correlation test was applied to the photoblock data and the InSAR data to insure that the photoblocks were adjusted appropriately.

<b>BLOCK</b>	<b>FIRST PHOTO</b>	<b>SECOND PHOTO</b>	<b>LOCAL COORD (0,0)</b>	<b>ROTATION</b>	<b>REFERENCE</b>
10-block WIS1	1986	1989	-138°10'00"W, -83°28'00"S (UpB)	-205	
10-block WIS2	1985	1986	-136°19'27" W, -83°12'56" S	187	Jackson (1991)
20-block	1986	1989	-138°10'00"W, -83°28'00"S (UpB)	180	
40-block	Jan. 22, 1985	Jan. 24, 1986	-147°31'38"W, -83°40'14"S		Whillans et al. (1987)

Table A1: Photoblock information

## APPENDIX B: MASS BALANCE RESULTS

The mass balance was calculated along each transect shown in Figure 4. The results are listed in Tables B1 and B2. In some cases where the area between the flux gates is small, the error is larger than the result. Tables B1 and B2 list all of the results, but in analyzing them, some gates are combined in order to get statistically different results.

In all calculations, the flux in and out of the gates is a product of the ice velocity, the ice thickness as determined by Shabtaie and Bentley (1988b) and the density of ice ( $917 \text{ kg/m}^3$ ).

Flow area	Tributary	<b>Fi</b> ( $10^{12}$ kg/yr)	<b>S</b> ( $10^6$ sq. m)	Accumulation rate (m/yr)	<b>Fs</b> ( $10^{10}$ kg/yr)	<b>Fin</b> ( $10^{12}$ kg/yr)	<b>Fout</b> ( $10^{12}$ kg/yr)	<b>Fnet</b> ( $10^{12}$ kg/yr)	<b>H</b> (cm/yr)
G1-G2	WIS1	12.13 (0.3)	855 (20)	0.12 (0.01)	9.41 (0.9)	12.22 (0.3)	12.20 (0.3)	0.02 (0.4)	3 (51)
G1-G2	WIS2	10.39 (0.2)	591 (6)	0.12 (0.01)	6.50 (0.7)	10.45 (0.2)	10.73 (0.2)	-0.28 (0.3)	-52 (55)
G1-G2	WIS	22.52 (0.3)	1446 (21)	0.12 (0.01)	15.91 (1.1)	22.67 (0.4)	22.93 (0.3)	-0.26 (0.5)	-20 (38)
G2-G3	WIS1	12.20 (0.3)	1885 (6)	0.11 (0.01)	19.0 (1.9)	12.39 (0.3)	12.07 (0.2)	0.32 (0.4)	19 (23)
G2-G3	WIS2	10.73 (0.2)	1827 (10)	0.11 (0.01)	18.43 (1.8)	10.9 (0.2)	10.96 (0.2)	-0.06 (0.3)	-3 (18)
G2-G3	WIS	22.93 (0.3)	3712 (12)	0.11 (0.01)	37.43 (2.6)	23.29 (0.4)	23.03 (0.5)	-0.26 (0.6)	7 (17)
G3-G4	WIS1	12.07 (0.2)	1105 (13)	0.10 (0.01)	11.15 (0.1)	12.18 (0.2)	12.63 (0.3)	-0.45 (0.3)	-44 (29)
G3-G4	WIS2	10.96 (0.2)	1268 (12)	0.10 (0.01)	12.79 (0.1)	11.09 (0.2)	12.57 (0.2)	-1.48 (0.3)	-127 (25)
G3-G4	WIS	23.03 (0.5)	2417 (15)	22.16 (2.2)	0.10 (0.01)	23.26 (0.5)	24.57 (0.19)	-1.32 (0.7)	-60 (31)

Table B1: Photoblock mass balance variables. **Fi** is the flux in through the up-stream gate ( $10^{12}$  kg/yr), **S** is the surface area in between the two flux gates ( $10^6$  m<sup>2</sup>), **Fs** is the flux through the ice surface (accumulation rate times the surface area) ( $10^{10}$  kg/yr), **Fin** is the sum of **Fi** and **Fs**, **Fout** is the flux out of the down-stream gate, **Fnet** is the net flux (**Fin** minus **Fout**) ( $10^{12}$  kg/yr), and **H** is the rate of thickness change (cm/yr).

Flow area	Tributary	<b>Fi</b> (10 <sup>12</sup> kg/yr)	<b>S</b> (10 <sup>6</sup> sq. m)	Accumulation (m/yr)	<b>Fs</b> (10 <sup>10</sup> kg/yr)	<b>Fin</b> (10 <sup>12</sup> kg/yr)	<b>Fout</b> (10 <sup>12</sup> kg/yr)	<b>Fnet</b> (10 <sup>12</sup> kg/yr)	<b>H</b> (cm/yr)
G0-G1	WIS1	12.22 (1.3)	2233 (10)	0.13 (0.01)	26.62 (2.6)	12.49 (0.6)	11.73 (0.8)	0.76 (1.0)	37 (49)
G0-G1	WIS2	9.39 (0.9)	2463 (10)	0.13 (0.01)	29.36 (3)	9.68 (0.9)	10.2 (0.5)	-0.5 (1.0)	-22 (44)
G0-G1	WIS	21.61 (1.6)	4696 (14)	0.13 (0.01)	55.98 (4)	22.17 (1.6)	21.93 (0.9)	0.24 (1.8)	6 (42)
G1-G2	WIS1	11.73 (0.8)	855 (20)	0.12 (0.01)	9.41 (0.9)	11.8 (0.8)	11.93 (0.6)	-0.13 (1.0)	-18 (128)
G1-G2	WIS2	10.2 (0.5)	591 (6)	0.12 (0.01)	6.50 (0.7)	10.26 (0.5)	10.46 (0.4)	-0.19 (0.6)	-31 (111)
G1-G2	WIS	21.93 (0.9)	1446 (21)	0.12 (0.01)	15.91 (1.1)	22.06 (0.9)	22.39 (0.7)	-0.33 (1.1)	-25 (83)
G2-G3	WIS1	11.93 (0.6)	1885 (6)	0.11 (0.01)	19.0 (1.9)	12.12 (0.7)	12.7 (0.4)	-0.58 (0.8)	-33 (46)
G2-G3	WIS2	10.46 (0.4)	1827 (10)	0.11 (0.01)	18.43 (1.8)	10.64 (0.4)	10.68 (0.3)	-0.04 (0.5)	-2 (30)
G2-G3	WIS	22.39 (0.7)	3712 (12)	0.11 (0.01)	37.43 (2.6)	22.76 (0.8)	23.39 (0.7)	-0.63 (1.0)	18 (30)
G3-G4	WIS1	12.7 (0.4)	1105 (13)	0.10 (0.01)	11.15 (0.1)	12.81 (0.4)	12.06 (0.4)	0.75 (0.5)	74 (49)
G3-G4	WIS2	10.68 (0.3)	1268 (12)	0.10 (0.01)	12.79 (0.1)	10.81 (0.3)	10.52 (0.3)	0.29 (0.4)	25 (34)
G3-G4	WIS	23.39 (0.7)	2417 (15)	0.10 (0.01)	22.16 (2.2)	23.61 (0.8)	22.56 (0.7)	1.05 (1.0)	32 (45)

Table B2: Photoblock mass balance variables. **Fi** is the flux in through the up-stream gate (10<sup>12</sup> kg/yr), **S** is the surface area in between the two flux gates (10<sup>6</sup> m<sup>2</sup>), **Fs** is the flux through the ice surface (accumulation rate times the surface area) (10<sup>10</sup> kg/yr), **Fin** is the sum of **Fi** and **Fs**, **Fout** is the flux out of the down-stream gate, **Fnet** is the net flux (**Fin** minus **Fout**) (10<sup>12</sup> kg/yr), and **H** is the rate of thickness change (cm/yr).